Quaternary Science Reviews
July 2022, Volume 287 Pages 107556 (14p.)
https://doi.org/10.1016/j.quascirev.2022.107556
https://archimer.ifremer.fr/doc/00773/88478/

Enhanced Carbonate Counter Pump and upwelling strengths in the Indian sector of the Southern Ocean during MIS 11

Brandon Margaux [1, 2, *], Duchamp-Alphonse Stéphanie [1], Michel Elisabeth [2], Landais Amaëlle [2], Isguder Gulay [2], Richard Patricia [2], Pige Nicolas [3], Bassinot Franck [2], Jaccard Samuel L. [4], Bartolini Annachiara [5]

[1] Université Paris-Saclay, CNRS, GEOPS, 91405, Orsay, France
[2] Université Paris-Saclay, CNRS, CEA, UVSQ, Laboratoire des Sciences du climat et de l'environnement, 91191, Gif-sur-Yvette, France
[3] Univ Lyon, UCBL, ENSL, UJM, CNRS, LGL-TPE, F-69622, Villeurbanne, France
[4] Institute of Earth Sciences, University of Lausanne, 1015, Lausanne, Switzerland
[5] Muséum National d'Histoire Naturelle, Département Origines & Évolution, CR2P MNHN, CNRS, Sorbonne Université, 8 rue Buffon CP38, 75005, Paris, France

* Corresponding author : Margaux Brandon, email address : margaux.brandon@locean.ipsl.fr

---

Abstract :

While numerous studies have highlighted the central role of Southern Ocean (SO) dynamics in modulating rapid increases in atmospheric CO2 concentrations during deglaciations, fewer studies have yet focused on the impact of the Biological Carbon Pump - and more specifically the Carbonate Counter Pump (CCP) - in contributing to increase the CO2 concentration in oceanic surface waters and thus, in the atmosphere. Here, we present micropaleontological (coccolith, planktonic foraminifera) and geochemical (CaCO3, CaXRF, δ13CN. pachyderma) constraints from sediment core MD04-2718 retrieved in the Polar Front Zone of the Indian Ocean covering the time interval spanning Marine Isotope Stage (MIS) 12 to MIS 10 (440,000–360,000 years). We compare our results with published records from the SO to reconstruct past changes in CCP and upwelling dynamics and understand their leverage on the ocean-atmosphere portioning of CO2. We demonstrate that the sharp increase in atmospheric pCO2 during Termination V was likely associated with enhanced deep-water ventilation in the SO, that promoted the release of previously sequestered CO2 to the ocean surface as the westerly wind belt and the frontal system migrated southwards. Enhanced CCP is observed later, during MIS 11, and is likely the consequence of higher sea surface temperature and higher nutrient availability due to the reinvigoration of SO upwelling leading to increased coccolith (and to a lesser degree, planktonic foraminifera) production and export. The low eccentricity signal recorded during MIS 11 might have additionally strengthened the CCP, exerting a specific control on Gephyrocapsa morphotypes. In addition to the strong global biological productivity and higher carbon storage on land, these synergistic mechanisms may have permitted to shape the distinctive 30 ka-long pCO2 plateau characteristic of MIS 11.

Highlights

► Multiproxy approach to reconstruct Carbonate Counter Pump strength and upwelling dynamics. ► Increase in pCO_2 during Termination V coincides with enhanced upwelling. ► Strong Carbonate Counter Pump during MIS 11 in the Indian Southern Ocean. ► Enhanced upwelling and Carbonate Counter Pump helped shape the pCO_2 plateau.

Keywords : Southern Ocean, Marine Isotope Stage 11, Coccolith, Planktonic foraminifera, Geochemistry, Carbonate Counter Pump, Upwelling, Atmospheric CO2 concentration

1. Introduction

The Earth's climate system of the past 800 000 years (800 ka) has been characterised by glacial-interglacial cycles that are tightly coupled to pCO_2 changes (Lüthi et al., 2008; Bereiter et al., 2015). Causes underlying these changes, especially in conjunction with deglaciations (glacial Terminations) that registered pCO_2 rises of about 50-100 ppm, are still under debate. It is recognised that complex, synergistic interactions involving changes in sea-ice cover, surface water stratification and marine productivity in the SO together with the dynamics of the westerly winds may have played a major role in modulating the efficiency of the physical and biological carbon pumps (François et al., 1997; Stephens and Keeling, 2000; Sigman and Boyle, 2000; Hodell et al., 2003; Toggweiler et al., 2006; Jaccard et al., 2013; Ferrari et al., 2014; Abelmann et al., 2015; Galbraith & Jaccard, 2015; Menviel et al., 2018; Gottschalk et al., 2019; Stein et al., 2020; Sigman et al., 2021). The reinvigoration of SO upwelling has been held responsible for a substantial part of the abrupt pCO_2 rise observed during Terminations (Hodell et al., 2003; Anderson et al., 2009; Skinner et al., 2010; Siani et al., 2013, Jaccard et al., 2016; Rae et al., 2018; Gottschalk et al., 2020; Sigman et al., 2021) while an increase in the efficiency of the Biological Carbon Pump (BCP) might have accounted for up to 40-50 ppmv CO_2 drawdown during glacial maxima (Hain et al., 2010; Martinez-Garcia et al., 2009; Jaccard et al., 2013). However, due to a lack of high-resolution primary productivity reconstructions and, more generally, to the scarcity of multiproxy approaches (Duncan et al., 2016; Duchamp-Alphonse et al., 2018), it remains difficult to apprehend the spatio-temporal patterns underpinning changes in the BCP and compare them to the SO upwelling dynamics to understand their impact on pCO_2. Furthermore, most of the studies aiming to reconstruct changes in the strength and efficiency of the BCP focus on the export of phytoplankton-derived organic carbon to the deep ocean (i.e., the Soft Tissue Pump (STP)) that directly lowers atmospheric CO_2 (Martin et al., 1990; Martinez-Garcia et al., 2009; Martinez-Garcia et al., 2014; Thöle et al., 2019). They typically overlook the export of phytoplankton- and zooplankton-derived calcium carbonate ($CaCO_3$), which raises surface water CO_2

(i.e., the CCP) (Baumann et al., 2004; Barker et al., 2006; Broecker and Clark, 2009; Salter et al., 2014; Rembauville et al., 2016), and contributes to the $CaCO_3$/organic carbon ratio in the biogenic particle flux to the sea-floor (namely the rain ratio), especially in the SO (Duchamp-Alphonse et al., 2018; Krumhardt et al., 2020). This omission may relate to the fact that calcareous phytoplankton is in part represented by coccoliths, which detailed analysis requires sophisticated tools such as SYRACO (SYstème de Reconnaissance Automatique des Coccolithes), a software using automated optical microscope that allows the robust determination of coccolith mass and thus, coccolithophore calcification rates, based on the optical properties (birefringence) of calcite under cross-polarized light (Beaufort et al., 2005; 2014). It is also probably linked to the lack of well-preserved carbonate fraction in sediment cores of the SO, making the reconstruction of biogenic carbonate export in the past challenging (Barker et al., 2006; Jaccard et al., 2013; Thöle et al., 2019).

Amongst the interglacials of the past 800 ka, MIS 11 is the longest (~30 ka) as well as one of the warmest (Tzedakis et al., 2022 and references therein). Following the cold glacial MIS 12, MIS 11 begins at the end of Termination V (TV), the first Termination recording high amplitude increases in both pCO_2 (~ 90 ppmv) (Bereiter et al., 2015; Nehrbass-Ahles et al., 2020) and Antarctic air temperatures (> 12°C) (Jouzel et al., 2007). MIS 11 occurs during an eccentricity minimum (Laskar et al., 2004) and coincides with strong global biosphere productivity (Brandon et al., 2020), a major phase in coral reef expansion (Husson et al., 2018), and a climax in coccolithophore (*Gephyrocapsa* sp.) production (Barker et al., 2006; Beaufort et al., 2022). Recent studies document the increase in coccolith abundances over this time interval in the Pacific and Atlantic sectors of the SO (Flores et al., 2003; Saavedra-Pellitero et al., 2017a; 2017b). However, no studies exist in the Indian sector of the SO yet, and none focus on the CCP and its impact on atmospheric pCO_2 based on combined coccolith and planktonic foraminifera carbonate export data.

Here, we provide coccolith and planktonic foraminifera abundance and mass from core MD04-2718 retrieved in the Indian sector of the SO. Using these data, we demonstrate the biogenic origin of the sedimentary $CaCO_3$ at this site and calibrate the carbonate signal to reconstruct high resolution changes in CCP strength across the time interval covering MIS 12 – MIS 10 (440-360 ka), including TV and MIS 11. Combined with reconstructed summer SST and $\delta^{13}C_{N.\ pachyderma}$ data obtained from the same core, ~~as well as~~ previously published micropaleontological and geochemical data from the Pacific and Atlantic sectors of the SO as well as geochemical data from EPICA Dome C (EDC), our study further highlights the synergistic contribution of changing global productivity and terrestrial carbon storage, SO ventilation and CCP strength on atmospheric CO_2 during this key period of the past 800 ka.

2. Regional oceanic setting

The SO is delimited by the Antarctic continent to the South and by the Subtropical front (STF) to the North (Fig. 1a). The eastward-flowing Antarctic Circumpolar Current (ACC) connects the Atlantic, Pacific and Indian sectors of the SO. This current, driven by Coriolis and the Southern Hemisphere westerlies, is characterised by the largest mass transport of all ocean currents, averaging 150 Sv ($10^6 m^3 s^{-1}$) in the Indian Ocean (Park et al., 2009). Its Northern and Southern Boundaries (NB and SB) are often delimited around 40°S and 60°S respectively, but their exact location depends on bottom topography (Sokolov and Rintoul, 2009, Park et al., 2019) and varies latitudinally (Freeman et al., 2016). Three hydrological fronts generally characterised by stronger flows, are defined in the ACC: the Subantarctic Front (SAF), the Polar Front (PF) and the Southern Antarctic Circumpolar Front (SACCF) (Fig. 1). They help defining the Subantarctic Zone (SAZ) between the STF and the SAF, the Polar Front Zone (PFZ) between the SAF and the PF, and the Antarctic Zone (AAZ) delimited by the PF to the North, and the SB to the South (Orsi et al., 1995, Park et al., 2019). Within the Indian sector of the SO, the Kerguelen Plateau that extends from ~ 46°S to 63°S and between ~ 62°E and 85°E, is the second largest submarine plateau in the world. Due to its great meridional extent and topography, it constitutes a major bathymetric constrain to the ACC flow and thus exerts a significant impact on both ACC transport and front patterns (Park et al., 2009; Sokolov and Rintoul, 2009). In this context, the PF is located alongside the southern coast of the Kerguelen archipelago (Park et al., 2014). The circulation in the Southern Ocean is also regulated by the upwelling of CO_2- and nutrient-rich Circumpolar Deep Waters (CDW) that resurface at the Antarctic divergence in the AAZ (Fig. 1c). These waters represent the source for the Subantarctic Mode Water (SAMW) and the Antarctic Intermediate Water (AAIW) that flow northward. Today, the change in the strength of upwelling affects the partitioning of CO_2 between the ocean subsurface and the atmosphere on decadal timescales (Lovenduski et al., 2008; Landschützer et al., 2015; Gruber et al, 2019).

In the SO, primary productivity is primarily steered by bottom-up control involving both physical and biogeochemical processes, which are spatially and temporally heterogeneous. Today, the presence/absence of sea ice together with the progressive temperature decrease polewards subdivide the SO into distinct provinces characterised by specific functional assemblages (Boyd, 2002; Constable et al., 2014). In ecosystems that remain ice-free throughout the year, i.e., within the Permanently Open Ocean Zone (POOZ), primary productivity is commonly co-limited by light and micronutrient availability (Boyd et al., 2002; Moore et al., 2013). While the residual surface ocean macronutrient concentrations in the SO are among the highest globally (Pollard et al., 2006) largely due to the large-scale upwelling of CDW at the Antarctic divergence, primary productivity is relatively low, owing to the scarcity of bioavailable iron (Fe) imposes on phytoplankton growth (Martin et al., 1990; Pollard et al., 2009). In all cases, phytoplankton that flourishes south of the PF is dominated by diatoms, with blooms generally occurring during austral summer (Rigual-Hernandez et al., 2015). Phytoplankton that thrives north of the PF is more heterogeneous and represented by nano- and picoplankton of different origins. One of the most striking patterns associated with phytoplankton in this area, is the significant coccolithophore blooms that occur during spring and summer between ~40 and ~60°S, and that forms the so-called Great Calcite Belt that enriches surface waters in $CaCO_3$ (Balch et al., 2011; 2016; Rembauville et al., 2016). Within the Indian sector of the SO, near the Kerguelen plateau, this Great Calcite Belt is observed in the PFZ (Smith et al., 2017) and the northern part of the AAZ (between Kerguelen and Heard and McDonald Islands) and may contribute ~ 60 to 85 % of the CCP (Blain et al., 2007; Rembauville et al., 2016; Smith et al., 2017; Rigual-Hernandez et al., 2020). Relatively high primary productivity may also be observed locally, near the PF and the Crozet and Kerguelen plateaus, where oceanic current and/or bottom topography enriches surface waters with iron (Blain et al., 2007; Sokolov and Rintoul, 2007; Pollard et al., 2009; Quéguiner et al., 2013; Tagliabue et al., 2014).

3. Material and methods

3.1 Material core

The 50-meter-long marine sediment core MD04-2718 (48°53,31S; 65°57,42E, 1428 m water depth) was retrieved from the NW flank of the Kerguelen Plateau in 2004, during the MD136/VIGO expedition aboard the R.V. Marion Dufresne (Fig. 1, Michel and Waelbroeck, 2017) within the PFZ. Surface water properties are largely controlled by CO_2- and nutrient- rich waters upwelling in the Antarctic Zone, that are advected northward by the Ekman transport. Sediment recovered at this site is primarily siliciclastic with alternations of nannofossil (calcareous) and diatom (opal) oozes. MIS 11 is clearly identifiable and represented by calcareous-rich ooze, between 11.5 and 13.1 m core depth.

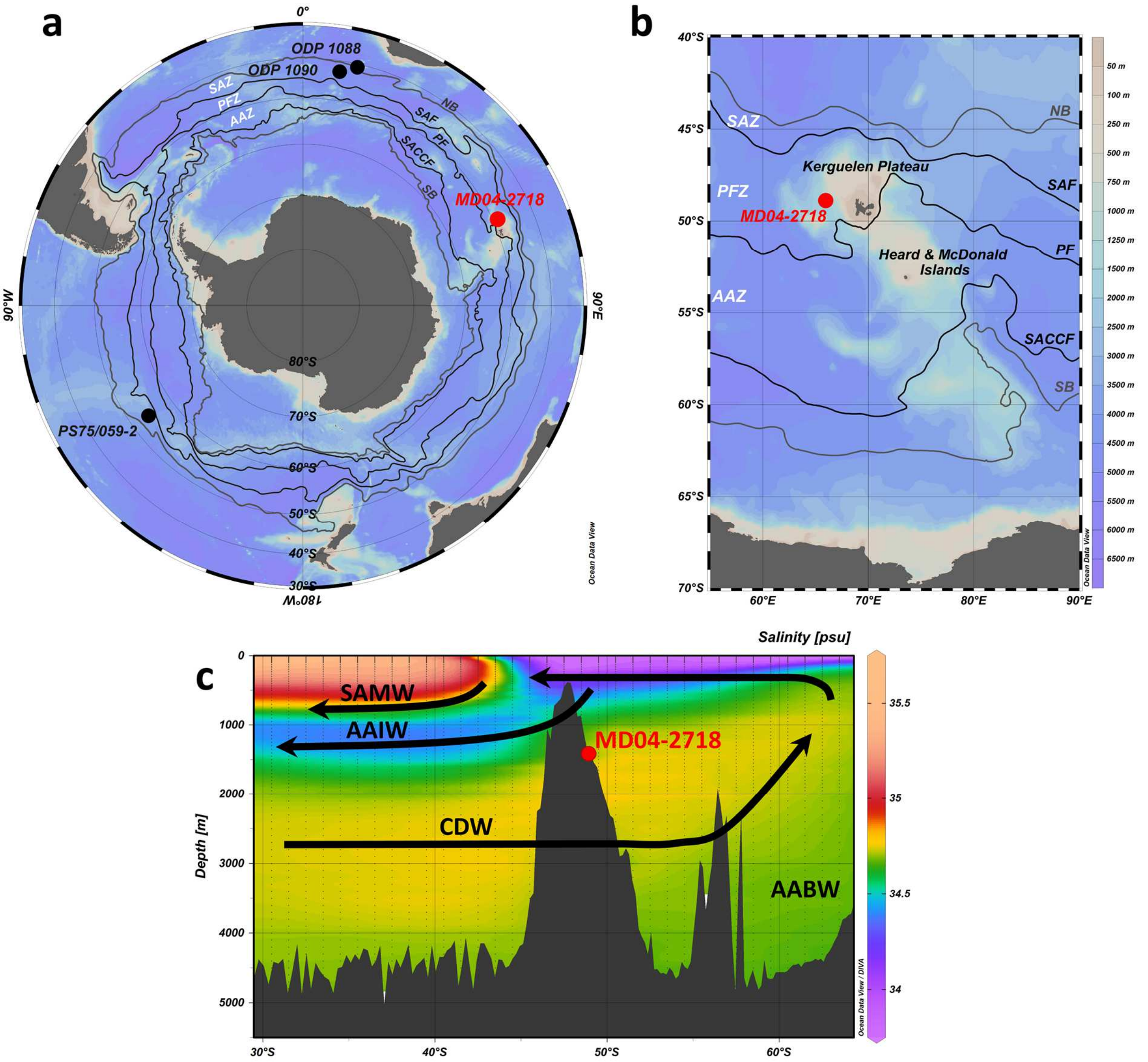

Figure 1 Core location and study area. **a, b** Location of the studied core (MD04-2718, red dot) as well as cores from previous studies (ODP sites 1088 and 1090 (Hodell et al., 2003) and PS75/059-2 (Saavedra-Pellitero et al., 2017a; 2017b) (black dots). Oceanic fronts are from Park et al. (2019). NB: Northern Boundary of the ACC, SAZ: Subantarctic Zone, SAF: Subantarctic Front, PFZ: Polar Front Zone, PF: Polar Front, AAZ: Antarctic Zone, SACCF: Southern Antarctic Circumpolar Front, SB: Southern Boundary of the ACC **.c** Salinity (psu) section at 66°E using WOA18 (Zweng et al., 2018) on ODV software (Schlitzer, 2018). SAMW: Subantarctic Mode Water, AAIW: Antarctic Intermediate Water, CDW: Circumpolar Deep Water, AABW: Antarctic Bottom Water.

3.2 Geochemical analyses

Planktonic foraminifera $\delta^{18}O$ and $\delta^{13}C$ compositions (expressed in ‰) were measured at the LSCE (Laboratoire des Sciences du Climat et de l'Environnement), based on 67 *Neogloboquadrina pachyderma* senestral (200-250 µm fraction, Supplementary Fig. 1) samples, subsampled every 3-4 cm between 11.03 and 13.3 m depth (except for 13.07, 13.10 and 13.13 m, which are barren of *N. pachyderma* s). For each sample, 30 specimens were hand-picked, cleaned using methanol, ultrasonicated, weighted, and analysed using an IRMS GV ISOPRIME mass spectrometer coupled with an extraction line. The measurements are reported versus the Vienna Pee Dee Belemnite standard (VPDB) with respect to NBS-19 standard, with a mean external reproducibility (1σ) for carbonate standards of ± 0.04 ‰ and 0.06 ‰ for $\delta^{13}C$ and $\delta^{18}O$, respectively. The reproducibility of isotopic measurements on *N. pachyderma* s. are 0.06 and 0.1 ‰, for $\delta^{13}C$ and $\delta^{18}O$, respectively.

High-resolution, relative sedimentary calcium (Ca) concentrations were measured every 1 cm using an Aavatech profiling X-ray Fluorescence (XRF) core scanner at ETH Zurich, Switzerland with a 10s integration at 10 kV and 500 µA. In parallel, sedimentary $CaCO_3$ concentrations were determined on 26 samples at GEOPS Laboratory with a ± 2 % precision, using the vacuum-gasometric technique described in Duchamp-Alphonse et al., (2018) where the amount of CO_2 degassed during the reaction of 100 mg ± 2 mg of dried sediments with 6N HCl is converted into $CaCO_3$ percentages. Comparison between Ca counts and discrete $CaCO_3$ contents show a highly significant statistical correlation (r^2=0.97), and Ca_{XRF} signal is therefore directly converted into $CaCO_3$ content (Jaccard et al., 2009; 2010; Duchamp-Alphonse et al., 2018; Supplementary Fig. 2).

3.3 Micropaleontological analyses

3.3.1 Coccoliths

Coccolith abundance and mass were determined at the GEOPS (GEOscience Paris Saclay) Laboratory. Smear slides were prepared for 68 samples, based on the protocol detailed in Duchamp-Alphonse et al., (2018), after Beaufort et al., (2014). For each sample, the abundance and mass of individual coccoliths (with an average of 6,172 coccoliths per sample (176 to 13,233)) were automatically determined with the help of the SYRACO software using a Leica DM6000B microscope. SYRACO detects and classifies most of the coccoliths (*Gephyrocapsa caribbeanica,* small *Gephyrocapsa*, *G. oceanica*, *G. muellerae, Calcidiscus leptoporus* and *Coccolitus pelagicus*) present on the slides. Coccolith mass was also directly obtained using SYRACO based on a quasi-linear relationship between their brightness (birefringence in grey scale) and their thickness under cross-polarized light. Because this method applies to coccoliths thinner than 1.55 µm, we interpret only thickness and mass data for *Gephyrocapsa* specimens, as C. *leptoporus* and *C. pelagicus* display third-order interferences. The presence of relatively large detrital particles may lead to an underestimation of small specimens including *Gephyrocapsa* sp. and an overestimation of larger ones including *C. pelagicus*. To correct for these potential biases, the abundance of each morphotype was verified manually on 18 samples covering the full spectrum of coccolith abundance observed from MIS 12 to

MIS 10. Visual counts were performed on the same view fields analysed by SYRACO and were compared to the results obtained by the software. *Gephyrocapsa* sp. abundances from SYRACO counts were calibrated using the correlation coefficients between the two datasets, while *C. pelagicus* abundances have been obtained visually for the entire sample set because of the confusion made by SYRACO between detrital particles and this species. *C. leptoporus* abundances did not differ significantly between SYRACO and visual counts were not corrected.

The number of coccoliths per gram of sediment (absolute coccolith abundance – ACA) was determined for each morphotype/species using the equation of Grelaud et al., (2009) as follows:

$$ACA = \frac{N_c * S_f}{N_o * S_o * W_s}$$

where N_c represents the total coccolith number per sample, S_f, the flat beaker area (3117 mm^2), N_o, the number of view fields (165), S_o, the view field area (0.01 mm^2) and W_s, the dry sediment weight.

The coccolith calcite mass per gram of sediment (per g. sed) was determined using the same equation, where Nc is replaced by Mc, that represents the coccolith calcite mass per view fields. *Gephyrocapsa* calcite mass (CM_{gephy}) was obtained based on the estimation of specimen abundance and mean mass as follows:

$$CM_{Gephy} = ACA * mean\ mass_{Gephy}$$

3.3.2 Planktonic foraminifera

The abundance and planktonic foraminifera species composition were determined at the LSCE with a binocular microscope, using the > 150 µm fraction of 57 samples ranging between 11.30 m and 13.3 m depth. For each sample, an average of 450 planktonic foraminifera were counted. The absolute planktonic foraminifera abundance (AFA) per gram of sediment was determined as follows:

$$AFA = \frac{N_f * 2^{split}}{W_{dry}}$$

where N_f represents the number of planktonic foraminifera counted per sample (> 300), split is the number of splits performed on the sediment before counting ($0 \leq split \leq 6$), and W_{dry}, the dry sediment sample weight.

The planktonic foraminifera calcite mass was determined at the LSCE using mean weights of the major planktonic foraminifera species from the >150 µm fraction. The foraminifera calcite mass is thus underestimated as it does not consider juveniles planktonic foraminifera or smaller species such as *G. uvula*. Yet the weight variations of this fraction are considered representative of the weight variations of the total planktic foraminifera fraction. The calcite mass produced by planktonic foraminifera, $CaCO_{3plank.foram}$, is (in mg/g):

$$CaCO_{3plank.foram} = \frac{(\sum_i (\sum_j m_{ji} * size_{ji}) * X_i) * AFA}{10^7}$$

Where m_{jj} represents the mean weight in size range j of specie I (in µg), $size_{ji}$ the percentage of population in size range j for specie i, and X_i the percentage of the specie i in the sample. The error on the mass will be:

$$\frac{1}{10^7} * (\sum_i X_i * (\sum_j size_{ji} * err_{m_{ij}} + \sum_j err_{size_{ji}} * m_{ij}) + \sum_i err_{X_i} * (\sum_j size_{ji} * m_{ji}))$$

where err is the error on each of the variables.

The size distribution, considering eight intervals (150-200 µm, 200-250 µm, 250-315 µm, 315-355 µm, 355-400 µm, 400-450 µm, 450-500 µm and >500 µm), and the mean weight for each size has been determined at six depths for the eight species representing > 99 % of the assemblage. The mean weight has been determined from 15 weighings of 1 to 4 individuals (to reach weight between 10 to 40 µg), to decrease the weight error to 19 % [$(1/(2(n-1))^{0.5}$]. The eight species include *Neogloboquadrina pachyderma* sinistral and dextral, *Globigerinita glutinata, Turborotalia quinqueloba, Globigerina bulloides, Globorotalia inflata, Globoratalia crassaformis and Globorotalia truncatilunoides*. We determine mean weights of : 3.55 ± 0.32 µg for *N. pachyderma*, 9.42 ± 2.15 µg for *G. bulloides*, 3.48 ± 0.42 for *G. glutinata*, 13.9 ± 2.37 µg for *G. crassaformis* and 22.4 ± 5.39 µg for *G. inflata*. We assumed a similar weight to *G. glutinata* for *T. quinqueloba*. For *G. truncatilunoides*, we assumed a mean weight similar to *G. crassaformis*. For *N. pachyderma*, 90 to 97 % of the population ranges in the minimum measured size range (150-200 µm), and between 71 to 100 % for *G. glutinata* and *T. quinqueloba*. For the other species the size range distribution varies with depth with the main size range varying from 150-200 µm to 250-315 µm for *G. bulloides*, *G. crassaformis* and *G. truncatulinoides* and from 150-200 µm to 315-355 µm for *G. inflata*. The error on the calcite mass of the planktonic foraminifera depends thus mainly on the error on the population fraction in the different size range for the larger species. The error on the calcite mass of the planktonic foraminifera also considers the variations in planktonic foraminifera weight and size with depth observed in the core, that can be linked with the changes in atmospheric CO_2 concentration (Barker and Elderfield, 2002; Moy et al., 2009; Henehan et al., 2017). For the 57 samples, the calcite mass of the planktonic foraminifera and its error have been calculated from the counted abundance of the different species and their mean size and mean weight calculated from the six depths. The error on this calcite mass varies from 26 to 57 % and is linearly linked with the abundance of *G. bulloides* (r^2= 0.91). Although large, the error remains negligible compared to the observed variations that are almost a factor of a thousand.

Summer SST estimates were determined on the same 57 samples as those used for planktonic foraminifera assemblages based on two independent approaches: the Modern Analog Technique and the percentage of *N. pachyderma* s. The former one relies on the use of a database of modern foraminifera assemblage (Haddam et al., 2016) and the PaleoAnalog software (Therón et al., 2004) to find the closest modern analogues for the fossil assemblage (Prell, 1985; Haddam et al., 2016). The latter one is based on the linear relation between SST and the percentage of *N. pachyderma* s. in the total planktonic foraminifera assemblage following the equation of Govin et al. (2009):

$$T°C\ (\%\ pachy\ s.) = -0.087\ (\%\ pachy\ s.) + 11.339$$

No SST could be determined between 13.13 and 13.07 m depth as the number of planktonic foraminifera was insufficient (<300) for a robust temperature estimate. During glacial periods the number of foraminifera per gram of sediment decreases drastically and, in these three levels, the >150 µm fraction contains almost exclusively ice rafted detritus and radiolarians.

4. Results

4.1 Geochemical signals

Planktonic foraminifera $\delta^{18}O$ values range between 2.2 ‰ and 3.8 ‰ (Fig. 2a). After a rapid decrease from 3.7 to 2.2 ‰ between 13.00 and 12.33 m, values gradually increase to reach around 3.6 ‰ at 11.33 m. The $\delta^{13}C$ signal ranges from 0.75 ‰ to 1.67 ‰ (Fig. 2b). $\delta^{13}C$ values are characterised by a slightly increasing plateau between 12.80 and 12.23 m and two sharp decreases to the minimum value of 0.8 ‰ from 13.23 to 13.03 m and from 11.57 to 11.33 m.

Sedimentary $CaCO_3$ concentrations range between 5 % and 99 % (Fig. 2c). Values never exceed 20 % between 13.30 and 13.10 m and between 11.30 and 11.03 m, while they average 85 % between 12.67 and 11.90 m. The most striking trends are observed between 13.10 and 12.66 m and 12.03 and 11.41 m, where $CaCO_3$ concentrations undergo a drastic increase to maximum values of 99 % at 12.65 m and a two-fold decreasing trend to reach minimum values of 7 % at 11.38.

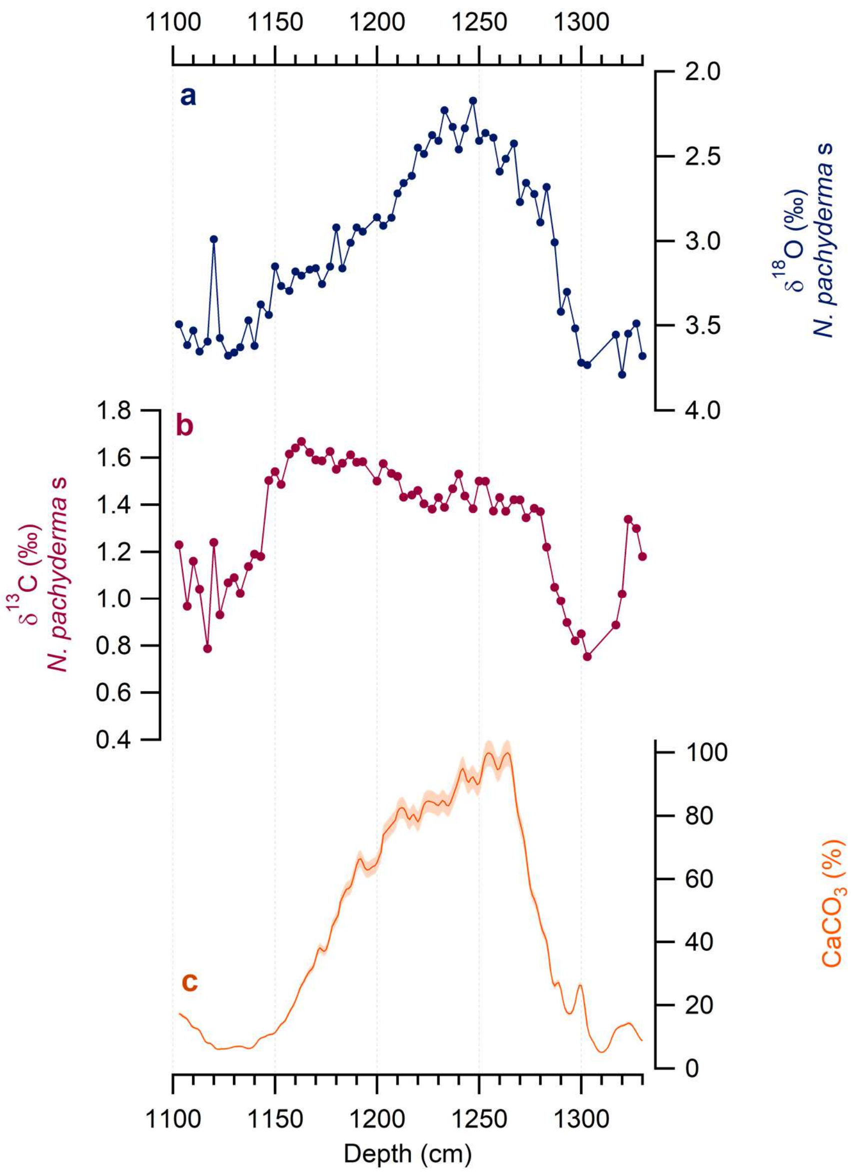

Figure 2 Bulk carbonate signals and stable isotope records of planktonic foraminifera *N. pachyderma s*. from sediment core MD04-2718. **a** $\delta^{18}O_{N.\ pachy\ s}$ (‰), **b** $\delta^{13}C_{N.\ pachy\ s}$ (‰), **c** $CaCO_3$ (%) derived from Ca_{XRF} signal, the envelope representing the error on the calculation of $CaCO_3$.

4.2 Micropaleontological signals

Coccolith assemblages are predominantly composed of *Gephyrocapsa* sp. i.e., specimens from the Noelaerhabdaceae family whose proportions exceed 98.5 %, reaching maximum values (99.9 %) between 12.87 and 11.33 m depths (Supplementary Fig. 3). *C. pelagicus* and *C. leptoporus* are present as well, but in much lower proportions. They are mainly represented by the subspecies *C. pelagicus* ssp. *braarudii* (10-14 µm) and *C. leptoporus* (5-8 µm) and range between 0 and 0.9 %, and 0 and 0.6 % of the assemblages, respectively. The number of total coccoliths per gram of sediments (per g. sed.) ranges from $0.017*10^9$ (at 13.10 m) to $40*10^9$ (at 12.10 m) and is mainly represented by the number of *Gephyrocapsa* sp. per g. sed. that fluctuates between $0.016*10^9$ and $40*10^9$ (Fig. 3b and 3c).

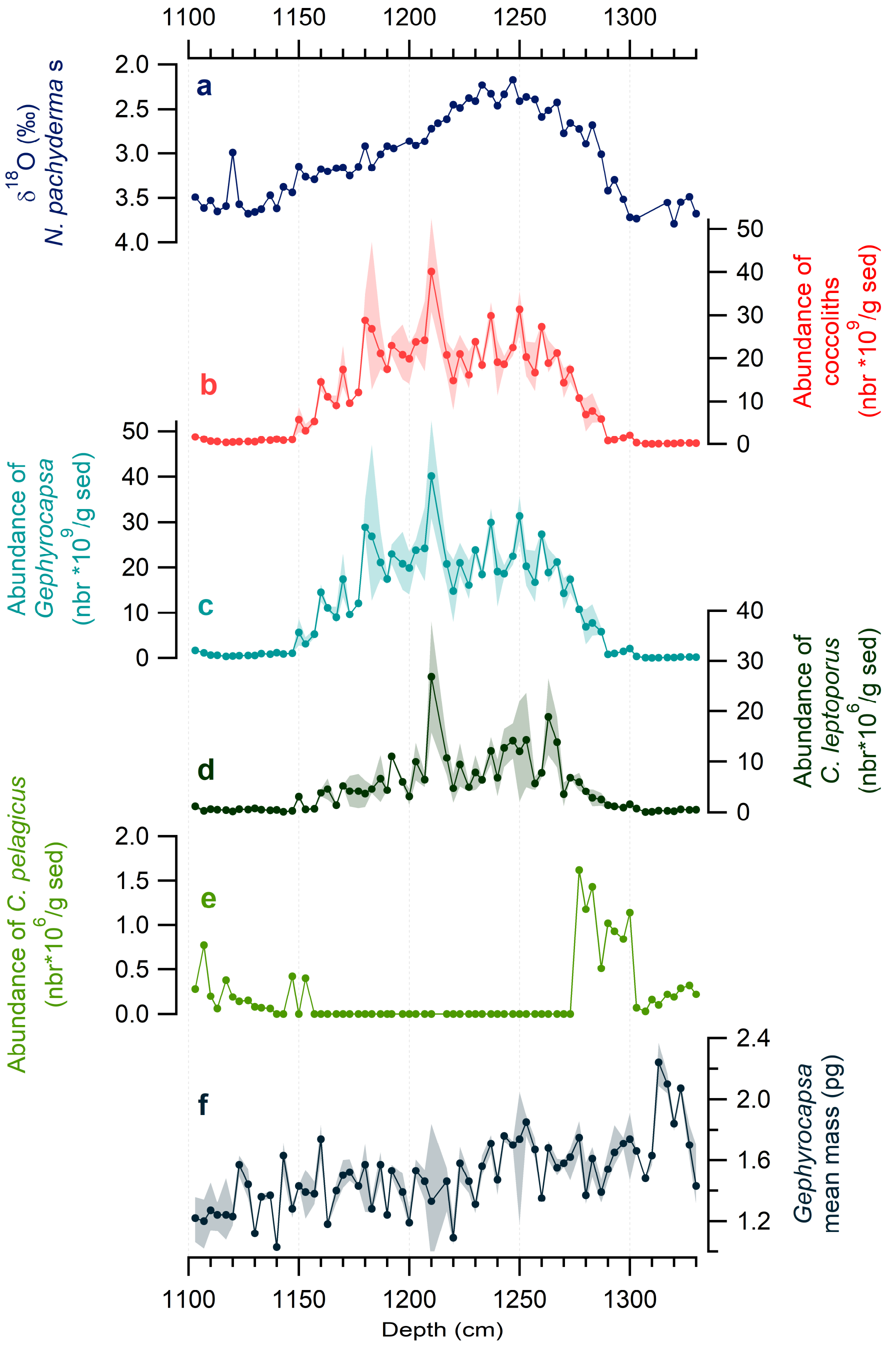

*Figure 3 Coccolith and $\delta^{18}O_{N.\ pachy\ s}$ signals between 1103 and 1330 cm of the sediment core MD04-2718. **a.** $\delta^{18}O_{N.\ pachy\ s}$ (‰), abundances of : **b** coccoliths (number of coccoliths$*10^9$ per g sed.), **c** Gephyrocapsa (number$*10^9$ per g sed.), **d** C. leptoporus (number$*10^6$ per g sed.),. **e** C. pelagicus (number$*10^6$ per g sed.), **f** Gephyrocapsa mean mass (pg). Envelopes in **b**, **c**, **d** and **f** show the error on SYRACO abundance for each specie and for Gephyrocapsa mean mass.*

After an increasing trend from 12.90 to 12.67 m, values show a plateau around $22.5*10^9$ specimens per g. sed. between 12.67 and 11.80 m and decreases to reach values as low as $0.35*10^9$ specimens per g. sed. at 11.17 m. *C. leptoporus* abundance fluctuates between $0.06*10^6$ and $21.6*10^6$ specimens per g. sed. and its distribution generally follows that of *Gephyrocapsa* sp. (and thus of total coccoliths), with an increasing trend between 13.07 and 12.67 cm followed by a long-term decreasing trend up to 11.47 m, interrupted by a transient a peak at 12.10 m (Fig. 3d). *C. pelagicus* abundance varies between 0 and $1.6*10^6$ coccoliths per g. sed (Fig. 3e). It is totally absent from the sediment between 12.73 and 11.54 m and is thus only present between 13.30 and 12.77 m and between 11.53 and 11.03 m, where it reaches values as high as 1.6 and $0.77*10^6$ specimens per g. sed, respectively. *Gephyrocapsa* sp. mean mass varies between 1.03 pg and 2.24 pg (Fig. 3f). After reaching maximum values (from 2.07 to 2.24 pg) between 13.23 and 13.13 m, data are consistent with a long-term decrease to reach minimum values around 11.40 m depth.

The planktonic foraminifera assemblages are mainly composed of *N. pachyderma* sinistral and *G. bulloides* with proportions ranging between 0 % and 99.8 % and between 0 and 75.1 %, respectively. The other species, represented by *G. glutinata*, *G. inflata*, *G. crassaformis*, *N. pachyderma* dextral and *T. quinqueloba* never exceed 6.8 %. (Supplementary Fig. 4). The total number of planktonic foraminifera fluctuates between 0 and $18.5*10^3$ specimens per g. sed (Fig. 4b). No specimen is found between 13.13 and 13.07 m, and the total abundance of planktonic foraminifera never exceeds $5.7*10^3$ between 13.30 and 12.9 m and between 11.5 and 11.3 m. Between 12.9 and 11.5 depth the number of *N. pachyderma* s. varies between 0.3 and $12.4*10^3$ specimens per g. sed (Fig. 4c), and significantly influences the total number of planktonic foraminifera which generally shows the same trends. Its abundance shows an overall plateau around $3*10^3$ specimens per g. sed, and 2 maxima ($12.4*10^3$ and $10.9*10^3$ specimens per g. sed) at 12.70 and 11.73 m, respectively. The number of *G. bulloides* fluctuates between 2.10 and $4.7*10^3$ specimens per g. sed (Fig. 4d). After reaching maximum value at 12.70 m, it depicts a long-term decreasing trend to the minimum abundance of 2.1 specimens per g. sed. at 11.3 m. The number of *N. pachyderma* d. varies between 0.14 and 548.6 specimens per g. sed. and follows the general same trends as those of total planktonic foraminifera and *N. pachyderma* s. (Fig. 4e). *G. glutinata* abundance ranges between 0.2 and 551 specimens per g. sed (Fig. 4f). It depicts rather scattered values with two peaks (512 and 551 specimens per g. sed.) at 12.70 and 12.33 m. *G. crassaformis* abundance fluctuates between 0 and 259.5 specimens per g. sed, with values averaging 150 specimens per g. sed between 12.70 and 12.13 m (Fig. 4g). *T. quinqueloba* abundance fluctuates between 0 and 219.4 specimens per g. sed, and no specific trend may be highlighted (Fig. 4h). Finally, *G. inflata* abundance ranges between 0 and 106 specimens per g. sed (Fig. 4i). Similarly, to *G. crassaformis*, no or very few specimens are found between 12.23 and 11.60 m.

The reconstructed summer SSTs fluctuate between 1.7 and 9.9 °C (Fig. 4j). The maximum temperature is reached after a drastic warming amounting ~8 °C between 13.27 and 13.00 m. It is followed by temperatures fluctuating between 4.6 and 8.3°C from 12.93 to 12.70 m, and a plateau around 8°C between 12.67 and 12.27 m. Then, summer SSTs gradually decrease and reach down to 3 °C between 12.03 and 11.30 m.

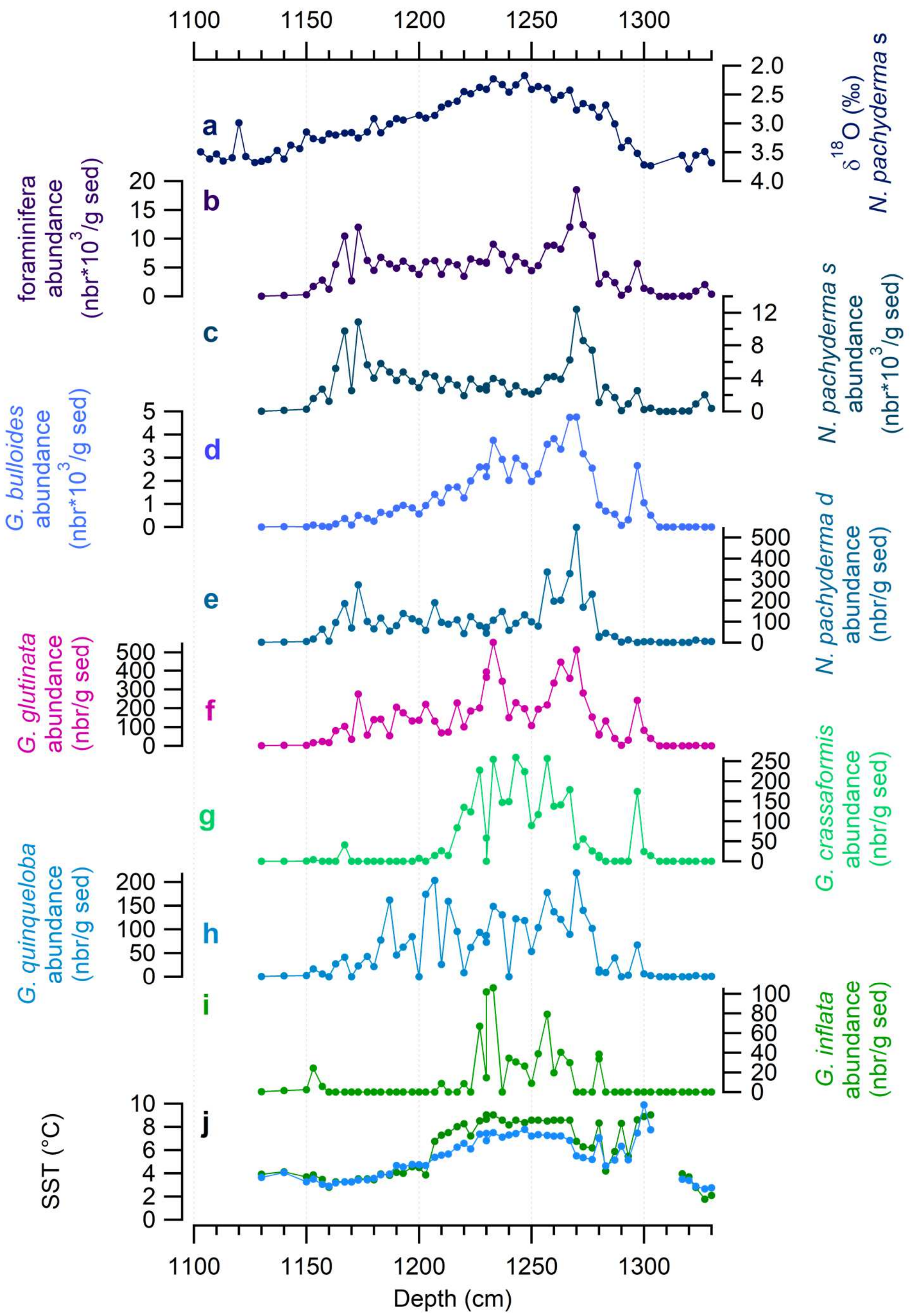

Figure 4 Planktonic foraminifera and $\delta^{18}O_{N.\ pachy\ s}$ signals between 1103 and 1330 cm of the sediment core MD04-2718. ***a*** *Signal of $\delta^{18}O_{N.\ pachy\ s}$ (‰),* ***b*** *Number of total planktonic foraminifera (per g sed.), Number (per g. of sed.) of:* ***c*** *N. pachyderma s.,* ***d*** *G. bulloides,* ***e*** *N. pachyderma d.,* ***f*** *G. glutinata,* ***g*** *G. crassaformis,* ***h*** *T. quinqueloba,* ***i*** *G. inflata,* ***j*** *Reconstructed summer SST (°C) using N. pachyderma s. percentages (blue curve) and based on Modern Analog Technique method (green curve).*

5. Age model

The age model of core MD04-2718 is based on the planktonic foraminifera $\delta^{18}O$ record and sedimentary $CaCO_3$ signal obtained on the uppermost 30 m of the core (Supplementary Fig. 5). These records helped identifying glacial-interglacial cycles and determining that the uppermost 20 m of the core covered the last 800 ka. It also allowed us to define the depth interval 13.00 to 11.00 m as representing the MIS 12 – MIS 10 time-interval and confirm our assumption that the nannofossil ooze between 11.5 and 13.1m was deposited during MIS 11 (see section 3.1). Numerous studies showed that the correlation between reconstructed SSTs in the Southern Ocean and air temperature reconstructed from Antarctic ice cores was helpful to better constrain sediment core age model (e.g., Pichon et al., 1992; Sowers et al. 1993; Waelbroeck et al., 1995; Thöle et al., 2019; Ai et al., 2020). Here, we used the record of δD of the EPICA Dome C ice core as a proxy for Antarctic surface temperature (Jouzel et al., 2007). As such, for the interval MIS 12 – 10, the age model of core MD04-2718 was refined based on the graphical alignment of our reconstructed summer SST with ~~record~~ ~~of~~the δD record on the AICC2012 timescale (Bazin et al., 2013), assuming an in-phase relationship (Fig. 5a). Using Analyseries software (Paillard et al., 1996), we set 5 tie points which helped us identifying the 11.03- 13.3 m core section as representing the time interval between 438.4 and 360.2 ka i.e., between the end of MIS 12 and the beginning of MIS 10. Over this period, the sedimentation rate averages 3.1 cm.ka^{-1} with lowest values (1 cm.ka^{-1}) being recorded during MIS 12, and highest ones (4.9 cm.ka^{-1}) being observed at the beginning of MIS 11 (Fig. 5b). Given these sedimentation rates, the temporal resolution of our record ranges from ~ 0.6 to 3.8 ka for micropaleontological and stable isotope data and of 0.2 to 2 ka for the $CaCO_3$ signal.

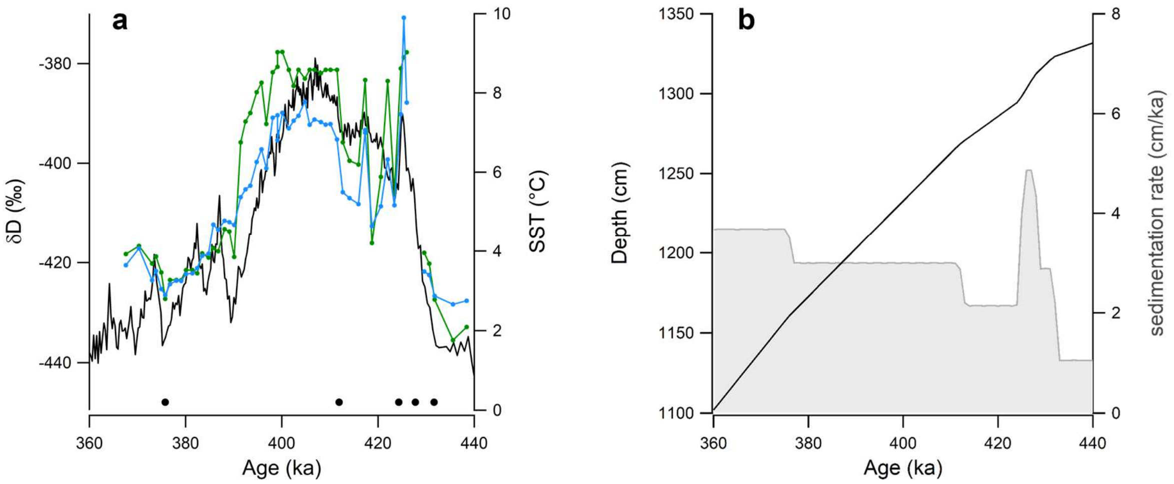

Figure 5 ***a*** *Age model of MD04-2718 based on the correlation between MD04-2718 summer SST reconstructions and EDC δD signal on AICC2012 timescale. Blue curve is the reconstructed summer SST using N. pachyderma s. percentages. Green curve is the reconstructed summer SST based on Modern Analog Technique method. Black curve is the δD measured in EDC ice core (Jouzel et al., 2007) on the AICC2012 timescale (Bazin et al., 2013). Black dots are the tie points between SST and δD* ***b*** *Estimated sedimentation rate of MD04-2718 core. Black curve represents the depth versus the calibrated age (ka BP on AICC2012) and the grey shaded area represent the variation of sedimentation rate with time.*

6. Discussion

6.1 $CaCO_3$ as a record of CCP strength

In pelagic environments of the SO, sedimentary carbonate concentration and/or coccolith abundances have been assumed to reflect biogenic carbonate export production - and by inference the strength of the CCP - based on the paradigm that in modern environments, and more particularly in the Great Calcite Belt, coccolithophores represent an important – if not dominant – part of exported mineralized organisms (Salter et al., 2014; Rembauville et al., 2016). However, the bulk sedimentary carbonate signal may include detrital or diagenetic phases and within the biogenic fraction, contributions of planktonic foraminifera and pteropods, the latter often considered negligible (Salter et al., 2014; Rembauville et al., 2016). Therefore, special attention must be devoted to assessing the significance of bulk sedimentary carbonate signals before making interpretations in terms of planktonic carbonate productivity and, by inference, of the CCP strength. It requires to carefully select the sedimentary cores that robustly reflect biogenic carbonate accumulation and to consider the potentially obfuscating impact of diagenesis.

Core MD07-2418 was retrieved at 1,428 m water depth i.e., well above the modern lysocline located at ~4,300 m (Kolla et al., 1976; Howard and Prell, 1994). The area only receives carbonate-free terrigenous material sourced from volcanic rocks of the Crozet and Kerguelen plateau (Nougier, 1970). Thus, the sedimented carbonate material directly relates to local biogenic carbonate production, for which the diagenetic overprint and potential detrital contribution are minimal. These assumptions are corroborated by Scanning Electron Microscopy (SEM) observations highlighting that the sedimentary carbonate fraction is predominantly constituted by very well-preserved foraminifera and coccoliths, sometimes represented as intact coccospheres (Fig. 6). In addition, we measured the relative proportion of fragmented planktonic foraminifera shells versus intact foraminifers, a well-characterised preservation index (Vazquez-Riveiros et al., 2010; Flores et al., 2003) (Supplementary Fig. 6). This foraminifera fragmentation index varies between 0 and 15.2 % with values higher than 3 % observed only between 426 and 417 ka. These results clearly indicate that planktonic foraminiferal preservation is generally good (Le and Shackleton, 1992).

Dissolution processes could result in differential sedimentary preservation in the coccolith assemblages as well, preferentially preserving resistant specimens. However, the assemblage is mainly constituted by well-preserved *Gephyrocapsa* sp., as seen on SEM observations. Furthermore, within this genus, small *Gephyrocapsa* sp. (<3 μm) follow the exact same trends as the larger ones, which suggests that differential dissolution does not significantly affect coccolith assemblages in sediments from core MD04-2718 (Supplementary Fig. 6).

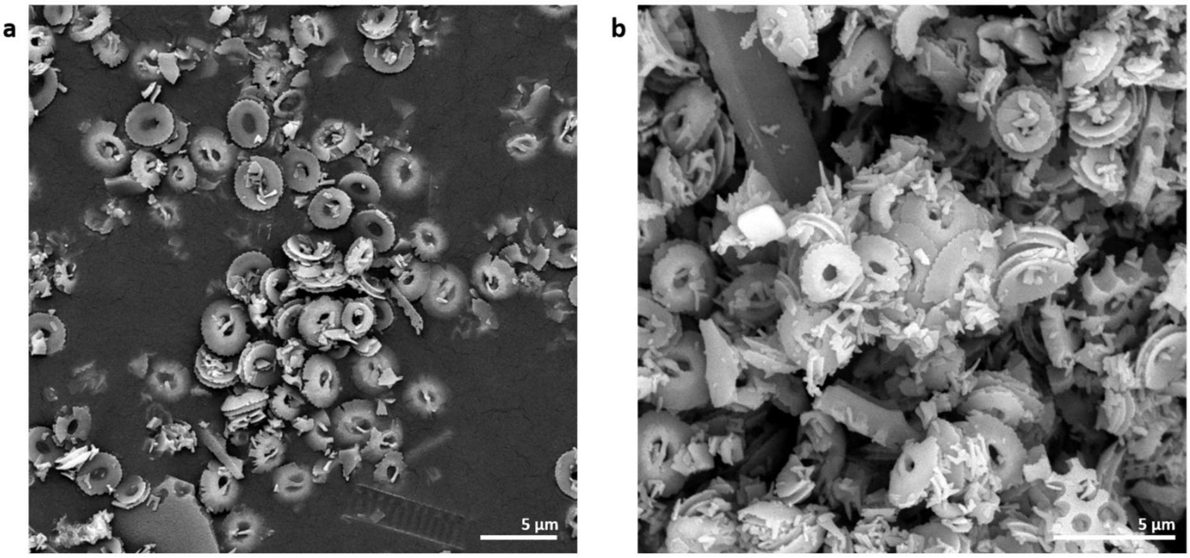

*Figure 6 Visual estimation of coccolith preservation of sediment core MD04-2718 based on Tescan VEGA II SEM observation (Museum National d'Histoire Naturelle, MNHN, Paris) showing good preservation **a** at 389.1 ka and **b** at 405.8 ka.*

At site MD04-2718, *Gephyrocapsa* calcite mass varies between 0.03 mg/g and 54.62 mg/g. The lowest values are recorded during MIS 12 (0.03 mg/g) and MIS 10 (0.43 mg/g) and the highest ones are documented during MIS 11. In detail, *Gephyrocapsa* calcite mass increases from 0.03 to 36.68 mg/g at the beginning of MIS 11, averages 30 mg/g during MIS 11, and decreases gradually from 382 ka to 372 ka to reach low values of 0.43 mg/g during glacial MIS 10. The *Gephyrocapsa* calcite mass record closely resembles the one of *Gephyrocapsa* sp. abundance, whereas no relationship may be observed with *Gephyrocapsa* mean mass (Fig. 7 and Supplementary Fig. 7). Moreover, while the variability in *Gephyrocapsa* sp. mean mass along the records are of a factor of two, the observed variations in abundance are more than a factor of two thousand. We therefore posit that changes in *Gephyrocapsa* calcite mass are mainly the consequence of changes in *Gephyrocapsa* abundance rather than in shell mean mass linked with shift in calcification or morphotypes~~.~~ The planktonic foraminifera (>150 µm) calcite mass varies between 0 and 93.9 mg/g. Briefly, it is characterised by null or low values during MIS 12 (< 7.2 mg/g) and MIS 10 (< 1.08 mg/g) and generally higher values during MIS 11 and the beginning of MIS 10 (> 20 mg/g). Maximum values are observed around 412.7 ka i.e., at the beginning of MIS 11. According to the significant linear correlation that exists between the *Gephyrocapsa* sp. + planktonic foraminifera calcite mass and sedimentary $CaCO_3$ content ($r^2 = 0.93$), it appears that both plankton groups constitute the major component of the biogenic carbonate signal. *Gephyrocapsa* sp. seems to have a relatively larger contribution on the sedimentary

$CaCO_3$ content as shown by its greater correlation to $CaCO_3$ ($r^2 = 0.89$) than planktonic foraminifera calcite mass itself ($r^2 = 0.83$) (Supplementary Fig. 2). Such results are consistent with the major control of coccoliths and more particularly morphotypes of the Noelaerhabdaceae family exert on PIC export today (Rembauville et al., 2016; Patil et al., 2020).

In the following, changes in the downcore $CaCO_3$ signal at site MD04-2718 will be interpreted in terms of changes in planktonic carbonate export, and by inference changes in CCP strength.

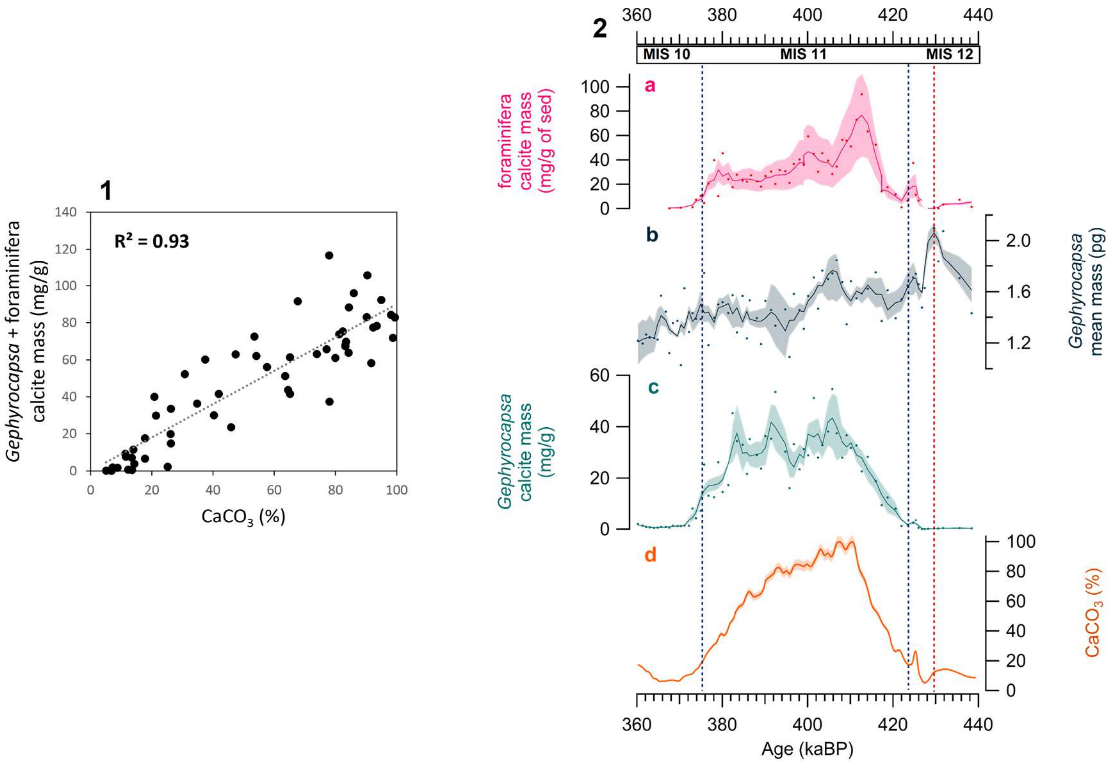

Figure 7 Origin of the carbonate fraction. ***1*** *Correlation between $CaCO_3$ and Gephyrocapsa + planktonic foraminifera calcite mass,* ***2 a*** *planktonic foraminifera calcite mass (mg/g),* ***b*** *Gephyrocapsa mean mass (pg),* ***c*** *Gephyrocapsa calcite mass (mg/g),* ***d*** *$CaCO_3$ (%). Smoothed curves use a three-point average using IGOR software. The shaded areas represent the error on the curve. The dotted blue lines represent the beginning and end of MIS 11 from right to left respectively, and the dotted red line represent the middle of the rising slope of CO_2 from glacial to interglacial.*

6.2 Increased CCP during MIS 11 as a response to the southward migration of westerly winds and ACC front positions

As represented by the variation in sedimentary $CaCO_3$ content, it appears that the CCP was strengthened during MIS 11 compared to MIS 12 and MIS 10 (Fig. 8). By analogy to the modern SO (Baumann et al., 1999; Zondervan et al., 2007) and the Pacific sector of the SAZ during MIS 12-MIS 10

(Schaefer et al., 2005; Ullermann, 2015; Saavedra-Pellitero et al., 2017a; 2017b), it is probable that such recorded pattern is related to substantial changes in SST and nutrient conditions. In addition to reconstructed SSTs, the abundances of *C. pelagicus* and *C. leptoporus* can be used to indirectly assess past changes in sea surface nutrient and temperature conditions. Indeed, while *C. pelagicus* seems to proliferate under colder conditions than *C. leptoporus* (Cobianchi et al., 2012), both these species appear to have affinities with relatively nutrient-rich waters (Andruleit, 1997; Balestra et al., 2004; Amore et al., 2012). This behaviour has been well documented on glacial/interglacial timescales in the SO (Flores et al., 1999; Findlay and Flores, 2000; Marino et al., 2009; Saavedra-Pellitero et al., 2017a; 2017b) to characteri~~z~~se frontal zone dynamics (Flores et al., 1999; Findlay and Giraudeau; 2000; Flores et al., 2003; Baumann et al., 2004; Malinverno et al., 2015; Marino et al., 2008; Saavedra-Pellitero et al., 2017a; 2017b). At core site MD04-2718, reconstructed SSTs range between ~2-4°C during glacial MIS 12 and MIS 10, and ~8°C during MIS 11 (Fig. 8). In parallel, relatively fertile conditions are inferred during TV and MIS 11 by the coccolith species *C. pelagicus* and *C. leptoporus* that peak between 426 and 415 ka and between 412 and 392 ka, respectively. The CCP was thus stronger during the relatively warm and nutrient-rich MIS 11 interglacial compared to the relatively cold and nutrient-depleted MIS 12 and MIS 10. The CCP trend shows however some temporal lag with the SST and nutrient records, highlighting other mechanisms in potentially regulating the variability of CCP strength. This is particularly obvious during TV (430-424 ka), when the CCP remains relatively weak despite drastic increases in SSTs and nutrient conditions. At that time, decreasing $\delta^{13}C_{N.pachyderma}$ values and increasing mean mass of *Gephyrocapsa* are recorded (Fig. 8). The rapid $\delta^{13}C$ decrease during the deglaciation is also documented in the South Pacific (Saavedra-Pellitero et al., 2017b) and South Atlantic (Hodell et al., 2003) (Fig. 8). This isotopic signal is consistent with the resumption of SO upwelling, which supplies abundant nutrients, previously sequestered in the ocean interior owing to greater water-column stratification, to the productive ocean surface (François et al., 1997; Spero et al., 2002; Adkins, 2013; Siani et al., 2013). Coeval increase in *Gephyrocapsa* mean mass has also been associated with increase in CO_2-rich upwelled waters in the SO (Duchamp-Alphonse et al., 2018). The reason behind these staggered and seemingly disconnected patterns could relate to the ecological competition between diatoms and coccolithophores in the SO. During glacial periods, favoured by higher iron (Fe) availability, diatom productivity outcompetes coccolithophore growth (Martin, 1990; Kohfeld et al., 2005; Martinez-Garcia et al., 2009; Thöle et al., 2019), and call for a weaker CCP. While the availability of Fe dwindled over deglacial periods, reinvigorated upwelling of nutrient-rich waters would have promoted diatom growth during Termination V. In such a scenario, we hypothesize that it is only during peak MIS 11 that silicic acid concentrations became too low, thereby limiting diatom growth (Sarmiento et al., 2004), and thus had the potential to favour coccolith production, enhancing the CCP. Overall, since the upwelled waters that (re)surface in the AAZ act under the forcing of the prevailing westerlies (Anderson et al., 2009; Lauderdale et al., 2013; Menviel et al., 2018), it is probable that winds migrated poleward between MIS 12 and MIS 11, concomitantly forcing the poleward migration of the entire frontal system (Flores and Sierro, 2007; Kemp et al., 2010; Saavedra-Pellitero et al., 2017a; 2017b). According to the reconstructed SST (< 8°C in mean) as well as the relatively low percentages of *C. leptoporus*, while close to the SAF, it is likely that site MD04-2718 remained in the PFZ. That is only around 390 ka, when SSTs decreased, that westerlies (along with the frontal system) might have shifted back to the North, leading to a decrease in the CCP.

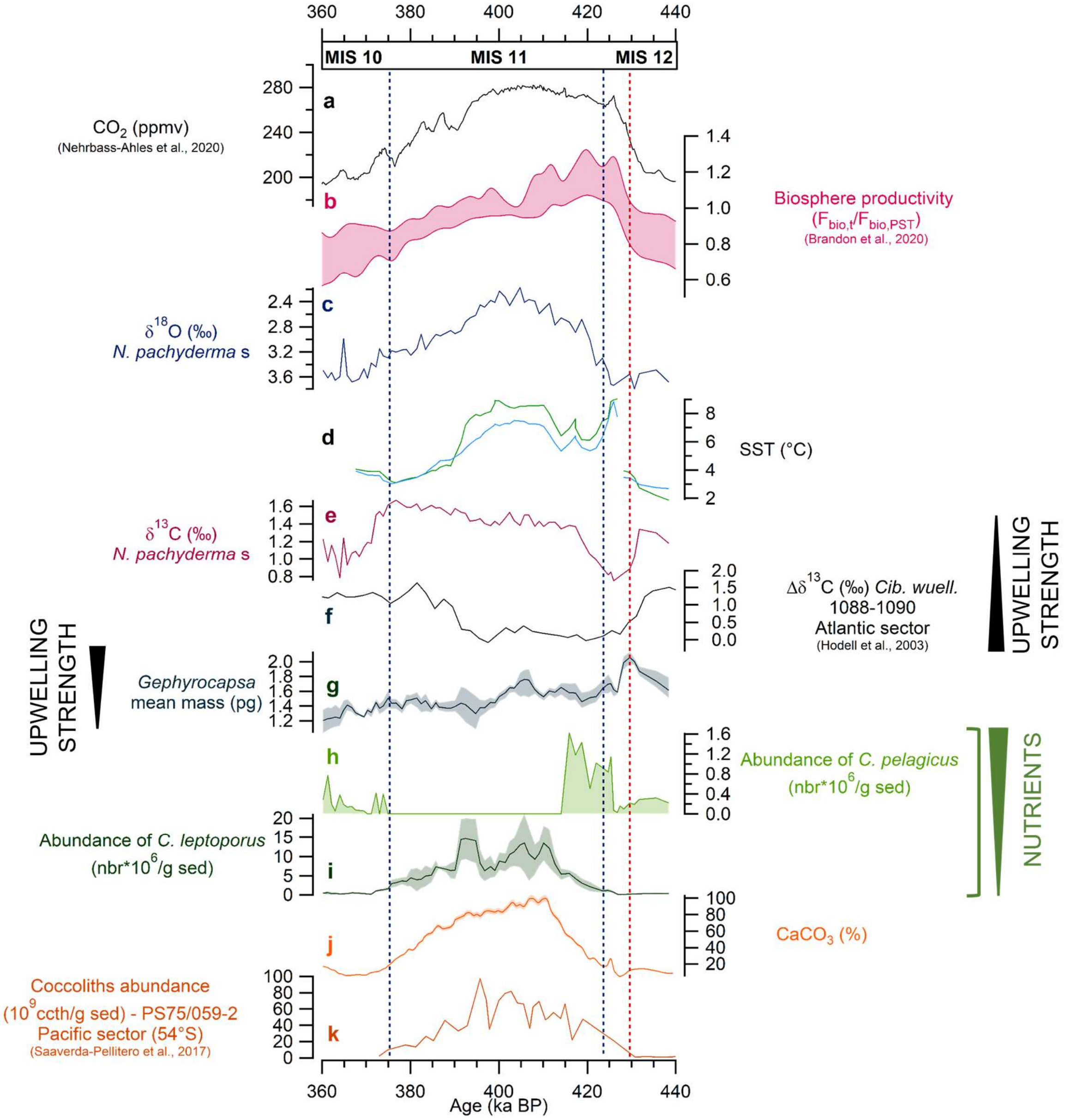

*Figure 8 Records of CCP and upwelling strengths in the SO and relation with variation of atmospheric CO_2 concentration.**a** CO_2 (ppm) (Nehrbass-Ahles et al., 2020), **b** Biopshere productivity (Fbio,t/Fbio,PST) (Brandon et al., 2020), **c** $\delta^{18}O$ of N. pachyderma s. from MD04-2718, **d** summer SST reconstructed using N. pachyderma s percentages (blue curve) and using Modern Analog Technique method (green curve), **e** $\delta^{13}C$ of N. pachyderma s. from MD04-2718, **f** $\Delta\delta^{13}C$ of benthic Cibicidoides wuellerstorfi from ODP Site 1088- ODP Site 1090 (Hodell et al., 2003), **g** Gephyrocapsa mean mass (pg), **h** C. pelagicus abundance (*10^6/g sed), **i** C. leptoporus abundance (*10^6/g sed), **j** $CaCO_3$ (%) derived from Ca_{XRF}, **k** PS75/059-2 Coccoliths abundance (10^9coccoliths/g of sediment, Saavedra-Pellitero et al., 2017b), showed on AICC2012 chronology.*

6.3 Increased CCP during TV and MIS 11 and its impact on atmospheric CO_2

The onset of deep-water ventilation following MIS 12 is recorded at ~432 ka, while the CCP starts to increase a few thousand years later, around 426 ka (Fig. 8). This distinct timing suggests that the rapid increase in atmospheric pCO_2 during Termination V was triggered, in part, by the reinvigoration of the SO upwelling early in the deglacial progression. Concomitant with the reinvigoration of SO upwelling, the increase in global biosphere productivity (Brandon et al., 2020) that reflects in part, an increase in vegetation cover and terrestrial carbon storage (Tzedakis et al., 2006; de Vernal and Hillaire-Marcel, 2008; Prokopenko et al., 2009; Melles et al., 2012; Kousis et al., 2018) has probably acted as a sink of atmospheric CO_2, thereby transiently buffering the impact of oceanic CO_2 degassing (Fig. 8). pCO_2 reached maximum concentration (up to ~ 282 ppm) during the second part of MIS 11, as the CCP functioned at maximum strength. Enhanced CCP in the SO contributed to reduce the efficiency of the BCP. Overall, enhanced *Gephyrocapsa* sp. export and burial both in the SO (Saavedra-Pellitero et al., 2017a; 2017b) and at low latitudes (Barker et al., 2006; Rickaby et al., 2007; Alvarez et al., 2010; Amore et al., 2012; Saavedra-Pellitero et al., 2019), would have led to a global increase in carbonate dissolution at the seafloor (Barker et al., 2006; Qin et al., 2018) and to a significant change in the global rain ratio, eventually impacting atmospheric pCO_2 (Sigman et al., 1998; Sigman and Boyle, 2000; Antia et al., 2001; Barker et al., 2006). This hypothesis warrants further investigations to fully quantify changes in the rain ratio and their impact on atmospheric pCO_2. From 398 ka to 381 ka, the gradual, ~35 ppm decrease in atmospheric pCO_2 coincided well with the rapid increase in benthic foraminifera $\Delta\delta^{13}C$ in the South Atlantic (Hodell et al., 2003), consistent with enhanced stratification of the SO and increased carbon storage in the ocean interior. The second part of atmospheric CO_2 drawdown during MIS 10 would be supported in part by the reduction in the strength of the CCP combined with a globally more efficient marine BCP.

At a global scale, the most striking pattern of MIS 11 relates to the low eccentricity context that is documented around 400 ka (Laskar et al., 2004). Low eccentricity, through the lengthening of the growing season, might have triggered an acme of primary producers such as *Gephyrocapsa* sp., at both high and low latitudes (Rickaby et al., 2007). One cannot exclude either that our record reflects the long-term cyclic Noelaerhabdaceae evolutionary pattern recently highlighted for the tropical area over the Pleistocene (Beaufort et al., 2022), with *Gephyrocapsa* blooms during MIS 11 being the consequence of reduced seasonality and phytoplankton niches. In all cases, we propose that, under this particularly low eccentricity context, enhanced terrestrial productivity and carbon storage on land, together with enhanced biological carbonate productivity and CCP strength in the SO may have contributed to shape the 30 ka-long CO_2 plateau characteristic of MIS 11.

7. Conclusion

Our study documents temporal variations in the strength of the CCP based on Southern Ocean sediments and their impact on atmospheric CO_2 concentrations over the period ranging between MIS 12 and MIS 10. First, using micropaleontological and geochemical data, we demonstrate that the sedimentary $CaCO_3$ signal robustly reflects the production and export of *Gephyrocapsa* sp. and (to a lesser degree) planktonic foraminifera and can therefore be used as a high-resolution proxy of the CCP. Second, using planktic foraminifera, *C. leptoporus* and *C. pelagicus* abundances combined with $\delta^{13}C$ of *N. pachyderma* s. from the same site, we reconstruct changes in sea surface temperature and nutrient conditions in conjunction with the regional upwelling dynamics, which are closely linked to the latitudinal migration of the westerly winds. Third, the combination of the results obtained in this study together with previous micropaleontological and geochemical data from literature allow us to highlight the sequence of events leading to the deglaciation and to understand the specific atmospheric pCO_2 pattern that characterises this key interval of the past. We show that the abrupt atmospheric CO_2 rise observed during TV is led by the reinvigoration of SO upwelling probably due to a poleward migration of the westerlies and ACC fronts, while the sustained CO_2 plateau observed during MIS 11 is the result of enhanced global primary productivity and increased CCP due to the exceptionally low eccentricity context.

Acknowledgments

This work benefited from founding from the INSU-LEFE-IMAGO program BIOCOD, from the European Research Council under the European Union H2020 Programme (H2020/20192024)/ ERC grant agreement no. 817493 ERC ICORDA as well as from the Institut Pierre Simon Laplace (IPSL). M.B. doctoral scholarship is supported by a public grant overseen by the French National research Agency

(ANR) as part of the « Investissement d'Avenir » program, through the "IDI 2017" project funded by the IDEX Paris-Saclay (grant ANR-11-IDEX-0003-02). S.L.J. acknowledges support from the Swiss National Science Foundation (grants PP00P2_144811 and PP00P2_163003). We thank Sylvain Pont and the Plateau technique de Microscopie Electronique (PtME, MNHN, Paris, France) for their assistance in providing SEM images, which helped for the estimation of the preservation of the carbonate fraction. We also thank Yvonne Hamann for instructions for the XRF core scanner at ETH, Zurich.

Data availability

Data will be made available in the Pangaea database prior to publication.

References

Abelmann, A., Gersonde, R., Knorr, G., Zhang, X., Chapligin, B., Maier, E., Esper, O., Friedrichsen, H., Lohmann, G., Meyer, H., Tiedemann, R., 2015. The seasonal sea-ice zone in the glacial Southern Ocean as a carbon sink. Nat Commun 6, 8136. https://doi.org/10.1038/ncomms9136

Adkins, J.F., 2013. The role of deep ocean circulation in setting glacial climates. Paleoceanography 28, 539–561. https://doi.org/10.1002/palo.20046

Ai, X.E., Studer, A.S., Sigman, D.M., Martínez-García, A., Fripiat, F., Thöle, L.M., Michel, E., Gottschalk, J., Arnold, L., Moretti, S., Schmitt, M., Oleynik, S., Jaccard, S.L., Haug, G.H., 2020. Southern Ocean upwelling, Earth's obliquity, and glacial-interglacial atmospheric CO_2 change. Science 370, 1348–1352. https://doi.org/10.1126/science.abd2115

Álvarez, M.C., Flores, J.A., Sierro, F.J., Molina-Cruz, A., 2010. Long-term upwelling evolution in tropical and equatorial Pacific during the last 800 kyr as revealed by coccolithophore assemblages. Geobios 8. https://doi.org/10.1016/j.geobios.2009.07.001

Amore, F.O., Flores, J.A., Voelker, A.H.L., Lebreiro, S.M., Palumbo, E., Sierro, F.J., 2012. A Middle Pleistocene Northeast Atlantic coccolithophore record: Paleoclimatology and paleoproductivity aspects. Marine Micropaleontology 90–91, 44–59. https://doi.org/10.1016/j.marmicro.2012.03.006

Anderson, R.F., Ali, S., Bradtmiller, L.I., Nielsen, S.H.H., Fleisher, M.Q., Anderson, B.E., Burckle, L.H., 2009. Wind-Driven Upwelling in the Southern Ocean and the Deglacial Rise in Atmospheric CO_2. Science 323, 1443–1448. https://doi.org/10.1126/science.1167441

Andruleit, H., 1997. Coccolithophore fluxes in the Norwegian-Greenland Sea: Seasonality and assemblage alterations. Marine Micropaleontology 31, 45–64. https://doi.org/10.1016/S0377-8398(96)00055-2

Antia, A.N., Koeve, W., Fischer, G., Blanz, T., Schulz-Bull, D., Schölten, J., Neuer, S., Kremling, K., Kuss, J., Peinert, R., Hebbeln, D., Bathmann, U., Conte, M., Fehner, U., Zeitzschel, B., 2001. Basin-wide particulate carbon flux in the Atlantic Ocean: Regional export patterns and potential for atmospheric CO_2 sequestration. Global Biogeochem. Cycles 15, 845–862. https://doi.org/10.1029/2000GB001376

Balch, W.M., Bates, N.R., Lam, P.J., Twining, B.S., Rosengard, S.Z., Bowler, B.C., Drapeau, D.T., Garley, R., Lubelczyk, L.C., Mitchell, C., Rauschenberg, S., 2016. Factors regulating the Great Calcite Belt in the Southern Ocean and its biogeochemical significance. Global Biogeochem. Cycles 30, 1124–1144. https://doi.org/10.1002/2016GB005414

Balch, W.M., Drapeau, D.T., Bowler, B.C., Lyczskowski, E., Booth, E.S., Alley, D., 2011. The contribution of coccolithophores to the optical and inorganic carbon budgets during the Southern Ocean Gas Exchange Experiment: New evidence in support of the “Great Calcite Belt” hypothesis. J. Geophys. Res. 116, C00F06. https://doi.org/10.1029/2011JC006941

Balestra, B., 2004. Coccolithophorids from the Southeast Greenland Margin (Northern North Atlantic): production, ecology and the surface sediment record. Micropaleontology 50, 23–34. https://doi.org/10.2113/50.Suppl_1.23

Barker, S., Archer, D., Booth, L., Elderfield, H., Henderiks, J., Rickaby, R.E.M., 2006. Globally increased pelagic carbonate production during the Mid-Brunhes dissolution interval and the CO_2 paradox of MIS 11. Quaternary Science Reviews 25, 3278–3293. https://doi.org/10.1016/j.quascirev.2006.07.018

Barker, S., Elderfield, H., 2002. Foraminiferal Calcification Response to Glacial-Interglacial Changes in Atmospheric CO_2. Science 297, 833–836. https://doi.org/10.1126/science.1072815

Baumann, K.-H., Böckel, B., Frenz, M., 2004. Coccolith contribution to South Atlantic carbonate sedimentation, in: Thierstein, H.R., Young, J.R. (Eds.), Coccolithophores. Springer Berlin Heidelberg, Berlin, Heidelberg, pp. 367–402. https://doi.org/10.1007/978-3-662-06278-4_14

Baumann, K.-H., Čepek, M., Kinkel, H., 1999. Coccolithophores as Indicators of Ocean Water Masses, Surface-Water Temperature, and Paleoproductivity — Examples from the South Atlantic, in: Fischer, G., Wefer, G. (Eds.), Use of Proxies in Paleoceanography. Springer Berlin Heidelberg, Berlin, Heidelberg, pp. 117–144. https://doi.org/10.1007/978-3-642-58646-0_4

Bazin, L., Landais, A., Lemieux-Dudon, B., Toyé Mahamadou Kele, H., Veres, D., Parrenin, F., Martinerie, P., Ritz, C., Capron, E., Lipenkov, V., Loutre, M.-F., Raynaud, D., Vinther, B., Svensson, A., Rasmussen, S.O., Severi, M., Blunier, T., Leuenberger, M., Fischer, H., Masson-Delmotte, V., Chappellaz, J., Wolff, E., 2013. An optimized multi-proxy, multi-site Antarctic ice and gas orbital chronology (AICC2012): 120–800 ka. Clim. Past 9, 1715–1731. https://doi.org/10.5194/cp-9-1715-2013

Beaufort, L., 2005. Weight estimates of coccoliths using the optical properties (birefringence) of calcite. Micropaleontology 51, 289–297. https://doi.org/10.2113/gsmicropal.51.4.289

Beaufort, L., Barbarin, N., Gally, Y., 2014. Optical measurements to determine the thickness of calcite crystals and the mass of thin carbonate particles such as coccoliths. Nat Protoc 9, 633–642. https://doi.org/10.1038/nprot.2014.028

Beaufort, L., Bolton, C.T., Sarr, A.-C., Suchéras-Marx, B., Rosenthal, Y., Donnadieu, Y., Barbarin, N., Bova, S., Cornuault, P., Gally, Y., 2022. Cyclic evolution of phytoplankton forced by changes in tropical seasonality. Nature 601, 79–84. https://doi.org/doi.org/10.1038/s41586-021-04195-7

Bereiter, B., Eggleston, S., Schmitt, J., Nehrbass-Ahles, C., Stocker, T.F., Fischer, H., Kipfstuhl, S., Chappellaz, J., 2015. Revision of the EPICA Dome C CO_2 record from 800 to 600 kyr before present. Geophys. Res. Lett. 42, 542–549. https://doi.org/10.1002/2014GL061957

Blain, S., Quéguiner, B., Armand, L., Belviso, S., Bombled, B., Bopp, L., Bowie, A., Brunet, C., Brussaard, C., Carlotti, F., Christaki, U., Corbière, A., Durand, I., Ebersbach, F., Fuda, J.-L., Garcia, N., Gerringa, L., Griffiths, B., Guigue, C., Guillerm, C., Jacquet, S., Jeandel, C., Laan, P., Lefèvre, D., Lo Monaco, C., Malits, A., Mosseri, J., Obernosterer, I., Park, Y.-H., Picheral, M., Pondaven, P., Remenyi, T., Sandroni, V., Sarthou, G., Savoye, N., Scouarnec, L., Souhaut, M., Thuiller, D., Timmermans, K., Trull, T., Uitz, J., van Beek, P., Veldhuis, M., Vincent, D., Viollier, E., Vong, L., Wagener, T., 2007. Effect of natural iron fertilization on carbon sequestration in the Southern Ocean. Nature 446, 1070–1074. https://doi.org/10.1038/nature05700

Boyd, P.W., 2002. Environmental factors controlling phytoplankton processes in the Southern Ocean. J Phycol 38, 844–861. https://doi.org/10.1046/j.1529-8817.2002.t01-1-01203.x

Brandon, M., Landais, A., Duchamp-Alphonse, S., Favre, V., Schmitz, L., Abrial, H., Prié, F., Extier, T., Blunier, T., 2020. Exceptionally high biosphere productivity at the beginning of Marine Isotopic Stage 11. Nat Commun 11, 2112. https://doi.org/10.1038/s41467-020-15739-2

Broecker, W., Clark, E., 2009. Ratio of coccolith $CaCO_3$ to foraminifera $CaCO_3$ in late Holocene deep sea sediments. Paleoceanography 24. https://doi.org/10.1029/2009PA001731

Cobianchi, M., Luciani, V., Lupi, C., Mancin, N., Lirer, F., Pelosi, N., Trattenero, I., Bordiga, M., Hall, I.R., Sprovieri, M., 2012. Pleistocene biogeochemical record in the south-west Pacific Ocean (images site MD97-2114, Chatham Rise). J. Quaternary Sci. 27, 519–530. https://doi.org/10.1002/jqs.2542

Constable, A.J., Melbourne-Thomas, J., Corney, S.P., Arrigo, K.R., Barbraud, C., Barnes, D.K.A., Bindoff, L., Boyd, P.W., Brandt, A., Costa, D.P., Davidson, A.T., Ducklow, H.W., Emmerson, L., Gutt, J., Hindell, M.A., Hofmann, E.E., Iida, T., Jacob, S., Johnston, N.M., Kokubun, N., Koubbi, P., Lea, M.-A., Makhado, A., Massom, R.A., Meiners, K., Murphy, E.J., Nicol, S., Reid, K., Riddle, M.J., Rintoul, S.R., Jr, W.O.S., Southwell, C., Stark, J.S., Sumner, M., Takahashi, K.T., Trathan, P.N., Welsford, D.C., Westwood, K.J., Wienecke, B.C., Wolf, D., 2014. Climate change and Southern Ocean ecosystems I: how changes in physical habitats directly affect marine biota. Global Change Biology 23. https://doi.org/10.1111/gcb.12623

de Vernal, A., Hillaire-Marcel, C., 2008. Natural Variability of Greenland Climate, Vegetation, and Ice Volume During the Past Million Years. Science 320, 1622–1625. https://doi.org/10.1126/science.1153929

Duchamp-Alphonse, S., Siani, G., Michel, E., Beaufort, L., Gally, Y., Jaccard, S.L., 2018. Enhanced ocean-atmosphere carbon partitioning via the carbonate counter pump during the last deglacial. Nat Commun 9, 2396. https://doi.org/10.1038/s41467-018-04625-7

Duncan, B., Carter, L., Dunbar, G., Bostock, H., Neil, H., Scott, G., Hayward, B.W., Sabaa, A., 2016. Interglacial/glacial changes in coccolith-rich deposition in the SW Pacific Ocean: An analogue for a warmer world? Global and Planetary Change 144, 252–262. https://doi.org/10.1016/j.gloplacha.2016.08.001

Ferrari, R., Jansen, M.F., Adkins, J.F., Burke, A., Stewart, A.L., Thompson, A.F., 2014. Antarctic sea ice control on ocean circulation in present and glacial climates. Proceedings of the National Academy of Sciences 111, 8753–8758. https://doi.org/10.1073/pnas.1323922111

Findlay, C.S., Flores, J.A., 2000. Subtropical Front fluctuations south of Australia (45°09'S, 146°17'E) for the last 130 ka years based on calcareous nannoplankton. Marine Micropaleontology 40, 403–416. https://doi.org/10.1016/S0377-8398(00)00045-1

Findlay, C.S., Giraudeau, J., 2000. Extant calcareous nannoplankton in the Australian Sector of the Southern Ocean (austral summers 1994 and 1995). Marine Micropaleontology 40, 417–439. https://doi.org/10.1016/S0377-8398(00)00046-3

Flores, J.-A., Gersonde, R., Sierro, F.J., 1999. Pleistocene fluctuations in the Agulhas Current Retroflection based on the calcareous plankton record. Marine Micropaleontology 37, 1–22. https://doi.org/10.1016/S0377-8398(99)00012-2

Flores, J.-A., Marino, M., Sierro, F.J., Hodell, D.A., Charles, C.D., 2003. Calcareous plankton dissolution pattern and coccolithophore assemblages during the last 600 kyr at ODP Site 1089 (Cape Basin, South Atlantic): paleoceanographic implications. Palaeogeography, Palaeoclimatology, Palaeoecology 196, 409–426. https://doi.org/10.1016/S0031-0182(03)00467-X

Flores, J.-A., Sierro, F.J., 2007. Pronounced mid-Pleistocene southward shift of the Polar Front in the Atlantic sector of the Southern Ocean. Deep Sea Research Part II: Topical Studies in Oceanography 54, 2432–2442. https://doi.org/10.1016/j.dsr2.2007.07.026

François, R., Altabet, M.A., Yu, E.-F., Sigman, D.M., Bacon, M.P., Frank, M., Bohrmann, G., Bareille, G., Labeyrie, L.D., 1997. Contribution of Southern Ocean surface-water stratification to low atmospheric CO_2 concentrations during the last glacial period. Nature 389, 929–935. https://doi.org/10.1038/40073

Freeman, N.M., Lovenduski, N.S., Gent, P.R., 2016. Temporal variability in the Antarctic Polar Front (2002-2014). J. Geophys. Res. Oceans 121, 7263–7276. https://doi.org/10.1002/2016JC012145

Galbraith, E.D., Jaccard, S.L., 2015. Deglacial weakening of the oceanic soft tissue pump: global constraints from sedimentary nitrogen isotopes and oxygenation proxies. Quaternary Science Reviews 109, 38–48. https://doi.org/10.1016/j.quascirev.2014.11.012

Gottschalk, J., Battaglia, G., Fischer, H., Frölicher, T.L., Jaccard, S.L., Jeltsch-Thömmes, A., Joos, F., Köhler, P., Meissner, K.J., Menviel, L., Nehrbass-Ahles, C., Schmitt, J., Schmittner, A., Skinner, L.C., Stocker, T.F., 2019. Mechanisms of millennial-scale atmospheric CO_2 change in numerical model simulations. Quaternary Science Reviews 220, 30–74. https://doi.org/10.1016/j.quascirev.2019.05.013

Gottschalk, J., Michel, E., Thöle, L.M., Studer, A.S., Hasenfratz, A.P., Schmid, N., Butzin, M., Mazaud, A., Martínez-García, A., Szidat, S., Jaccard, S.L., 2020. Glacial heterogeneity in Southern Ocean carbon storage abated by fast South Indian deglacial carbon release. Nat Commun 11, 6192. https://doi.org/10.1038/s41467-020-20034-1

Govin, A., Michel, E., Labeyrie, L., Waelbroeck, C., Dewilde, F., Jansen, E., 2009. Evidence for northward expansion of Antarctic Bottom Water mass in the Southern Ocean during the last glacial inception. Paleoceanography 24, n/a-n/a. https://doi.org/10.1029/2008PA001603

Grelaud, M., Beaufort, L., Cuven, S., Buchet, N., 2009. Glacial to interglacial primary production and El Niño-Southern Oscillation dynamics inferred from coccolithophores of the Santa Barbara Basin. Paleoceanography 24, n/a-n/a. https://doi.org/10.1029/2007PA001578

Gruber, N., Clement, D., Carter, B.R., Feely, R.A., van Heuven, S., Hoppema, M., Ishii, M., Key, R.M., Kozyr, A., Lauvset, S.K., Lo Monaco, C., Mathis, J.T., Murata, A., Olsen, A., Perez, F.F., Sabine, C.L., Tanhua, T., Wanninkhof, R., 2019. The oceanic sink for anthropogenic CO_2 from 1994 to 2007. Science 363, 1193–1199. https://doi.org/10.1126/science.aau5153

Haddam, N.A., Michel, E., Siani, G., Cortese, G., Bostock, H.C., Duprat, J.M., Isguder, G., 2016. Improving past sea surface temperature reconstructions from the Southern Hemisphere oceans using planktonic foraminiferal census data. Paleoceanography 31, 822–837. https://doi.org/10.1002/2016PA002946

Hain, M.P., Sigman, D.M., Haug, G.H., 2010. Carbon dioxide effects of Antarctic stratification, North Atlantic Intermediate Water formation, and subantarctic nutrient drawdown during the last ice age: Diagnosis and synthesis in a geochemical box model. Global Biogeochem. Cycles 24, GB4032. https://doi.org/10.1029/2010GB003790

Henehan, M.J., Evans, D., Shankle, M., Burke, J.E., Foster, G.L., Anagnostou, E., Chalk, T.B., Stewart, J.A., Alt, C.H.S., Durrant, J., Hull, P.M., 2017. Size-dependent response of foraminiferal calcification to seawater carbonate chemistry. Biogeosciences 14, 3287–3308. https://doi.org/10.5194/bg-14-3287-2017

Hodell, D.A., Venz, K.A., Charles, C.D., Ninnemann, U.S., 2003. Pleistocene vertical carbon isotope and carbonate gradients in the South Atlantic sector of the Southern Ocean. Geochem. Geophys. Geosyst. 4, 1–19. https://doi.org/10.1029/2002GC000367

Howard, W.R., Prell, W.L., 1994. Late Quaternary $CaCO_3$ production and preservation in the Southern Ocean: Implications for oceanic and atmospheric carbon cycling. Paleoceanography 9, 453–482. https://doi.org/10.1029/93PA03524

Husson, L., Pastier, A.-M., Pedoja, K., Elliot, M., Paillard, D., Authemayou, C., Sarr, A.-C., Schmitt, A., Cahyarini, S.Y., 2018. Reef Carbonate Productivity During Quaternary Sea Level Oscillations. Geochem. Geophys. Geosyst. 19, 1148–1164. https://doi.org/10.1002/2017GC007335

Jaccard, S.L., Galbraith, E.D., Martínez-García, A., Anderson, R.F., 2016. Covariation of deep Southern Ocean oxygenation and atmospheric CO_2 through the last ice age. Nature 530, 207–210. https://doi.org/10.1038/nature16514

Jaccard, S.L., Galbraith, E.D., Sigman, D.M., Haug, G.H., 2010. A pervasive link between Antarctic ice core and subarctic Pacific sediment records over the past 800kyrs. Quaternary Science Reviews 29, 206–212. https://doi.org/10.1016/j.quascirev.2009.10.007

Jaccard, S.L., Galbraith, E.D., Sigman, D.M., Haug, G.H., Francois, R., Pedersen, T.F., Dulski, P., Thierstein, H.R., 2009. Subarctic Pacific evidence for a glacial deepening of the oceanic respired carbon pool. Earth and Planetary Science Letters 277, 156–165. https://doi.org/10.1016/j.epsl.2008.10.017

Jaccard, S.L., Hayes, C.T., Martinez-Garcia, A., Hodell, D.A., Anderson, R.F., Sigman, D.M., Haug, G.H., 2013. Two Modes of Change in Southern Ocean Productivity Over the Past Million Years. Science 339, 1419–1423. https://doi.org/10.1126/science.1227545

Jouzel, J., Masson-Delmotte, V., Cattani, O., Dreyfus, G., Falourd, S., Hoffmann, G., Minster, B., Nouet, J., Barnola, J.M., Chappellaz, J., Fischer, H., Gallet, J.C., Johnsen, S., Leuenberger, M., Loulergue, L., Luethi, D., Oerter, H., Parrenin, F., Raisbeck, G., Raynaud, D., Schilt, A., Schwander, J., Selmo, E., Souchez, R., Spahni, R., Stauffer, B., Steffensen, J.P., Stenni, B., Stocker, T.F., Tison, J.L., Werner, M., Wolff, E.W., 2007. Orbital and Millennial Antarctic Climate Variability over the Past 800,000 Years. Science 317, 793–796. https://doi.org/10.1126/science.1141038

Kemp, A.E.S., Grigorov, I., Pearce, R.B., Naveira Garabato, A.C., 2010. Migration of the Antarctic Polar Front through the mid-Pleistocene transition: evidence and climatic implications. Quaternary Science Reviews 29, 1993–2009. https://doi.org/10.1016/j.quascirev.2010.04.027

Kohfeld, K.E., 2005. Role of Marine Biology in Glacial-Interglacial CO_2 Cycles. Science 308, 74–78. https://doi.org/10.1126/science.1105375

Kolla, V., Bé, A.W.H., Biscaye, P.E., 1976. Calcium carbonate distribution in the surface sediments of the Indian Ocean. J. Geophys. Res. 81, 2605–2616. https://doi.org/10.1029/JC081i015p02605

Kousis, I., Koutsodendris, A., Peyron, O., Leicher, N., Francke, A., Wagner, B., Giaccio, B., Knipping, M., Pross, J., 2018. Centennial-scale vegetation dynamics and climate variability in SE Europe during Marine Isotope Stage 11 based on a pollen record from Lake Ohrid. Quaternary Science Reviews 190, 20–38. https://doi.org/10.1016/j.quascirev.2018.04.014

Krumhardt, K.M., Long, M.C., Lindsay, K., Levy, M.N., 2020. Southern Ocean Calcification Controls the Global Distribution of Alkalinity. Global Biogeochem. Cycles 34. https://doi.org/10.1029/2020GB006727

Landschützer, P., Gruber, N., Haumann, F.A., Rödenbeck, C., Bakker, D.C.E., van Heuven, S., Hoppema, M., Metzl, N., Sweeney, C., Takahashi, T., Tilbrook, B., Wanninkhof, R., 2015. The reinvigoration of the Southern Ocean carbon sink. Science 349, 1221–1224. https://doi.org/10.1126/science.aab2620

Laskar, J., Robutel, P., Joutel, F., Gastineau, M., Correia, A.C.M., Levrard, B., 2004. A long-term numerical solution for the insolation quantities of the Earth. A&A 428, 261–285. https://doi.org/10.1051/0004-6361:20041335

Lauderdale, J.M., Garabato, A.C.N., Oliver, K.I.C., Follows, M.J., Williams, R.G., 2013. Wind-driven changes in Southern Ocean residual circulation, ocean carbon reservoirs and atmospheric CO_2. Clim Dyn 41, 2145–2164. https://doi.org/10.1007/s00382-012-1650-3

Le, J., Shackleton, N.J., 1992. Carbonate Dissolution Fluctuations in the Western Equatorial Pacific During the Late Quaternary. Paleoceanography 7, 21–42. https://doi.org/10.1029/91PA02854

Lovenduski, N.S., Gruber, N., Doney, S.C., 2008. Toward a mechanistic understanding of the decadal trends in the Southern Ocean carbon sink. Global Biogeochem. Cycles 22, n/a-n/a. https://doi.org/10.1029/2007GB003139

Lüthi, D., Le Floch, M., Bereiter, B., Blunier, T., Barnola, J.-M., Siegenthaler, U., Raynaud, D., Jouzel, J., Fischer, H., Kawamura, K., Stocker, T.F., 2008. High-resolution carbon dioxide concentration record 650,000–800,000 years before present. Nature 453, 379–382. https://doi.org/10.1038/nature06949

Malinverno, E., Triantaphyllou, M.V., Dimiza, M.D., 2015. Coccolithophore assemblage distribution along a temperate to polar gradient in the West Pacific sector of the Southern Ocean (January 2005). Micropaleontology 61, 489–506.

Marino, M., Maiorano, P., Lirer, F., 2008. Changes in calcareous nannofossil assemblages during the Mid-Pleistocene Revolution. Marine Micropaleontology 69, 70–90. https://doi.org/10.1016/j.marmicro.2007.11.010

Marino, M., Maiorano, P., Lirer, F., Pelosi, N., 2009. Response of calcareous nannofossil assemblages to paleoenvironmental changes through the mid-Pleistocene revolution at Site 1090 (Southern Ocean). Palaeogeography, Palaeoclimatology, Palaeoecology 280, 333–349. https://doi.org/10.1016/j.palaeo.2009.06.019

Martin, J.H., 1990. Glacial-interglacial CO_2 change: The iron hypothesis. Paleoceanography 5, 1–13.

Martínez-Garcia, A., Rosell-Melé, A., Geibert, W., Gersonde, R., Masqué, P., Gaspari, V., Barbante, C., 2009. Links between iron supply, marine productivity, sea surface temperature, and CO_2 over the last 1.1 Ma. Paleoceanography 24, n/a-n/a. https://doi.org/10.1029/2008PA001657

Martinez-Garcia, A., Sigman, D.M., Ren, H., Anderson, R.F., Straub, M., Hodell, D.A., Jaccard, S.L., Eglinton, T.I., Haug, G.H., 2014. Iron Fertilization of the Subantarctic Ocean During the Last Ice Age. Science 343, 1347–1350. https://doi.org/10.1126/science.1246848

Melles, M., Brigham-Grette, J., Minyuk, P.S., Nowaczyk, N.R., Wennrich, V., DeConto, R.M., Anderson, P.M., Andreev, A.A., Coletti, A., Cook, T.L., Haltia-Hovi, E., Kukkonen, M., Lozhkin, A.V., Rosen, P., Tarasov, P., Vogel, H., Wagner, B., 2012. 2.8 Million Years of Arctic Climate Change from Lake El'gygytgyn, NE Russia. Science 337, 315–320. https://doi.org/10.1126/science.1222135

Menviel, L., Spence, P., Yu, J., Chamberlain, M.A., Matear, R.J., Meissner, K.J., England, M.H., 2018. Southern Hemisphere westerlies as a driver of the early deglacial atmospheric CO_2 rise. Nat Commun 9, 2503. https://doi.org/10.1038/s41467-018-04876-4

Michel, E., Waelbroeck, C., 2017. MD 136/VIGO à bord du R/V Marion Dufresne. La Réunion 3 janvier 2004–La Réunion 9 février 2004. Les Rapports de Campagnes à la Mer.

Moore, C.M., Mills, M.M., Arrigo, K.R., Berman-Frank, I., Bopp, L., Boyd, P.W., Galbraith, E.D., Geider, R.J., Guieu, C., Jaccard, S.L., Jickells, T.D., La Roche, J., Lenton, T.M., Mahowald, N.M., Marañón, E., Marinov, I., Moore, J.K., Nakatsuka, T., Oschlies, A., Saito, M.A., Thingstad, T.F., Tsuda, A., Ulloa, O., 2013. Processes and patterns of oceanic nutrient limitation. Nature Geosci 6, 701–710. https://doi.org/10.1038/ngeo1765

Moy, A.D., Howard, W.R., Bray, S.G., Trull, T.W., 2009. Reduced calcification in modern Southern Ocean planktonic foraminifera. Nature Geosci 2, 276–280. https://doi.org/10.1038/ngeo460

Nehrbass-Ahles, C., Shin, J., Schmitt, J., Bereiter, B., Joos, F., Schilt, A., Schmidely, L., Silva, L., Teste, G., Grilli, R., Chappellaz, J., Hodell, D., Fischer, H., Stocker, T.F., 2020. Abrupt CO_2 release to the atmosphere under glacial and early interglacial climate conditions. Science 369, 1000–1005. https://doi.org/10.1126/science.aay8178

Nougier, J., 1970. Contribution à l'étude géologique et géomorphologique des îles Kerguelen (Terres Australes et Antarctiques Françaises). Com. natl. Fr. Rech. Antarct. 27, 246P.

Orsi, A.H., Whitworth, T., Nowlin, W.D., 1995. On the meridional extent and fronts of the Antarctic Circumpolar Current. Deep Sea Research Part I: Oceanographic Research Papers 42, 641–673. https://doi.org/10.1016/0967-0637(95)00021-W

Paillard, D., Labeyrie, L., Yiou, P., 1996. Macintosh Program performs time-series analysis. Eos, Transactions American Geophysical Union 77, 379–379. https://doi.org/10.1029/96EO00259

Park, Y., Durand, I., Kestenare, E., Rougier, G., Zhou, M., d'Ovidio, F., Cotté, C., Lee, J., 2014. Polar Front around the Kerguelen Islands: An up-to-date determination and associated circulation of surface/subsurface waters. J. Geophys. Res. Oceans 119, 6575–6592. https://doi.org/10.1002/2014JC010061

Park, Y. -H., Park, T., Kim, T. -W., Lee, S. -H., Hong, C. -S., Lee, J. -H., Rio, M. -H., Pujol, M. -I., Ballarotta, M., Durand, I., Provost, C., 2019. Observations of the Antarctic Circumpolar Current Over the Udintsev Fracture Zone, the Narrowest Choke Point in the Southern Ocean. J. Geophys. Res. Oceans 124, 4511–4528. https://doi.org/10.1029/2019JC015024

Park, Y.-H., Vivier, F., Roquet, F., Kestenare, E., 2009. Direct observations of the ACC transport across the Kerguelen Plateau. Geophys. Res. Lett. 36, L18603. https://doi.org/10.1029/2009GL039617

Patil, S.M., Mohan, R., Shetye, S.S., Gazi, S., Choudhari, P., Jafar, S., 2020. Interannual changes of austral summer coccolithophore assemblages and southward expanse in the Southern Indian Ocean. Deep Sea Research Part II: Topical Studies in Oceanography 178, 104765. https://doi.org/10.1016/j.dsr2.2020.104765

Pichon, J.-J., Labeyrie, L.D., Bareille, G., Labracherie, M., Duprat, J., Jouzel, J., 1992. Surface water temperature changes in the high latitudes of the southern hemisphere over the Last Glacial-Interglacial Cycle. Paleoceanography 7, 289–318. https://doi.org/10.1029/92PA00709

Pollard, R., Tréguer, P., Read, J., 2006. Quantifying nutrient supply to the Southern Ocean. J. Geophys. Res. 111, C05011. https://doi.org/10.1029/2005JC003076

Pollard, R.T., Salter, I., Sanders, R.J., Lucas, M.I., Moore, C.M., Mills, R.A., Statham, P.J., Allen, J.T., Baker, A.R., Bakker, D.C.E., Charette, M.A., Fielding, S., Fones, G.R., French, M., Hickman, A.E., Holland, R.J., Hughes, J.A., Jickells, T.D., Lampitt, R.S., Morris, P.J., Nédélec, F.H., Nielsdóttir, M., Planquette, H., Popova, E.E., Poulton, A.J., Read, J.F., Seeyave, S., Smith, T., Stinchcombe, M., Taylor, S., Thomalla, S., Venables, H.J., Williamson, R., Zubkov, M.V., 2009. Southern Ocean deep-water carbon export enhanced by natural iron fertilization. Nature 457, 577–580. https://doi.org/10.1038/nature07716

Prell, W.L., 1985. Stability of low-latitude sea-surface temperatures: an evaluation of the CLIMAP reconstruction with emphasis on the positive SST anomalies. U.S. Dep of Energy 60.

Prokopenko, A.A., Bezrukova, E.V., Khursevich, G.K., Solotchina, E.P., Kuzmin, M.I., Tarasov, P.E., 2010. Climate in continental interior Asia during the longest interglacial of the past 500 000 years: the new MIS 11 records from Lake Baikal, SE Siberia. Clim. Past 18.

Qin, B., Li, T., Xiong, Z., Algeo, T.J., Jia, Q., 2018. Deep-Water Carbonate Ion Concentrations in the Western Tropical Pacific Since the Mid-Pleistocene: A Major Perturbation During the Mid-Brunhes. J. Geophys. Res. Oceans 123, 6876–6892. https://doi.org/10.1029/2018JC014084

Quéguiner, B., 2013. Iron fertilization and the structure of planktonic communities in high nutrient regions of the Southern Ocean. Deep Sea Research Part II: Topical Studies in Oceanography 90, 43–54. https://doi.org/10.1016/j.dsr2.2012.07.024

Rae, J.W.B., Burke, A., Robinson, L.F., Adkins, J.F., Chen, T., Cole, C., Greenop, R., Li, T., Littley, E.F.M., Nita, D.C., Stewart, J.A., Taylor, B.J., 2018. CO_2 storage and release in the deep Southern Ocean on millennial to centennial timescales. Nature 562, 569–573. https://doi.org/10.1038/s41586-018-0614-0

Rembauville, M., Meilland, J., Ziveri, P., Schiebel, R., Blain, S., Salter, I., 2016. Planktic foraminifer and coccolith contribution to carbonate export fluxes over the central Kerguelen Plateau. Deep Sea Research Part I: Oceanographic Research Papers 111, 91–101. https://doi.org/10.1016/j.dsr.2016.02.017

Rickaby, R.E.M., Bard, E., Sonzogni, C., Rostek, F., Beaufort, L., Barker, S., Rees, G., Schrag, D.P., 2007. Coccolith chemistry reveals secular variations in the global ocean carbon cycle? Earth and Planetary Science Letters 253, 83–95. https://doi.org/10.1016/j.epsl.2006.10.016

Rigual Hernández, A.S., Trull, T.W., Nodder, S.D., Flores, J.A., Bostock, H., Abrantes, F., Eriksen, R.S., Sierro, F.J., Davies, D.M., Ballegeer, A.-M., Fuertes, M.A., Northcote, L.C., 2020. Coccolithophore biodiversity controls carbonate export in the Southern Ocean. Biogeosciences 17, 245–263. https://doi.org/10.5194/bg-17-245-2020

Rigual-Hernández, A.S., Trull, T.W., Bray, S.G., Closset, I., Armand, L.K., 2015. Seasonal dynamics in diatom and particulate export fluxes to the deep sea in the Australian sector of the southern Antarctic Zone. Journal of Marine Systems 142, 62–74. https://doi.org/10.1016/j.jmarsys.2014.10.002

Saavedra-Pellitero, M., Baumann, K.-H., Gallagher, S.J., Sagawa, T., Tada, R., 2019. Paleoceanographic evolution of the Japan Sea over the last 460 kyr – A coccolithophore perspective. Marine Micropaleontology 152, 101720. https://doi.org/10.1016/j.marmicro.2019.01.001

Saavedra-Pellitero, M., Baumann, K.-H., Lamy, F., Köhler, P., 2017a. Coccolithophore variability across Marine Isotope Stage 11 in the Pacific sector of the Southern Ocean and its potential impact on the carbon cycle. Paleoceanography 32, 864–880. https://doi.org/10.1002/2017PA003156

Saavedra-Pellitero, M., Baumann, K.-H., Ullermann, J., Lamy, F., 2017b. Marine Isotope Stage 11 in the Pacific sector of the Southern Ocean; a coccolithophore perspective. Quaternary Science Reviews 158, 1–14. https://doi.org/10.1016/j.quascirev.2016.12.020

Salter, I., Schiebel, R., Ziveri, P., Movellan, A., Lampitt, R., Wolff, G.A., 2014. Carbonate counter pump stimulated by natural iron fertilization in the Polar Frontal Zone. Nature Geoscience 7, 885–889. https://doi.org/10.1038/NGEO2285

Sarmiento, J.L., Gruber, N., Brzezinski, M.A., Dunne, J.P., 2004. High-latitude controls of thermocline nutrients and low latitude biological productivity. Nature 427, 56–60. https://doi.org/10.1038/nature02127

Schaefer, G., Rodger, J.S., Hayward, B.W., Kennett, J.P., Sabaa, A.T., Scott, G.H., 2005. Planktic foraminiferal and sea surface temperature record during the last 1 Myr across the Subtropical Front, Southwest Pacific. Marine Micropaleontology 54, 191–212. https://doi.org/10.1016/j.marmicro.2004.12.001

Schlitzer, R., 2018. Ocean Data View. https://odv.awi.de.

Siani, G., Michel, E., De Pol-Holz, R., DeVries, T., Lamy, F., Carel, M., Isguder, G., Dewilde, F., Lourantou, A., 2013. Carbon isotope records reveal precise timing of enhanced Southern Ocean upwelling during the last deglaciation. Nat Commun 4, 2758. https://doi.org/10.1038/ncomms3758

Sigman, D.M., Boyle, E.A., 2000. Glacial/interglacial variations in atmospheric carbon dioxide. Nature 407, 859–869. https://doi.org/10.1038/35038000

Sigman, D.M., Fripiat, F., Studer, A.S., Kemeny, P.C., Martínez-García, A., Hain, M.P., Ai, X., Wang, X., Ren, H., Haug, G.H., 2021. The Southern Ocean during the ice ages: A review of the Antarctic surface isolation hypothesis, with comparison to the North Pacific. Quaternary Science Reviews 254, 106732. https://doi.org/10.1016/j.quascirev.2020.106732

Sigman, D.M., McCorkle, D.C., Martin, W.R., 1998. The calcite lysocline as a constraint on glacial/interglacial low-latitude production changes. Global Biogeochem. Cycles 12, 409–427. https://doi.org/10.1029/98GB01184

Skinner, L.C., Fallon, S., Waelbroeck, C., Michel, E., Barker, S., 2010. Ventilation of the Deep Southern Ocean and Deglacial CO_2 Rise. Science 328, 1147–1151. https://doi.org/10.1126/science.1183627

Smith, H.E.K., Poulton, A.J., Garley, R., Hopkins, J., Lubelczyk, L.C., Drapeau, D.T., Rauschenberg, S., Twining, B.S., Bates, N.R., Balch, W.M., 2017. The influence of environmental variability on the biogeography of coccolithophores and diatoms in the Great Calcite Belt. Biogeosciences 14, 4905–4925. https://doi.org/10.5194/bg-14-4905-2017

Sokolov, S., Rintoul, S.R., 2009. Circumpolar structure and distribution of the Antarctic Circumpolar Current fronts: 1. Mean circumpolar paths. J. Geophys. Res. 114, C11018. https://doi.org/10.1029/2008JC005108

Sokolov, S., Rintoul, S.R., 2007. On the relationship between fronts of the Antarctic Circumpolar Current and surface chlorophyll concentrations in the Southern Ocean. J. Geophys. Res. 112, C07030. https://doi.org/10.1029/2006JC004072

Sowers, T., Bender, M., Labeyrie, L., Martinson, D., Jouzel, J., Raynaud, D., Pichon, J.J., Korotkevich, Y.S., 1993. A 135,000-year Vostok-SPECMAP common temporal framework. Paleoceanography 8, 737–766.

Spero, H.J., 2002. The Cause of Carbon Isotope Minimum Events on Glacial Terminations. Science 296, 522–525. https://doi.org/10.1126/science.1069401

Stein, K., Timmermann, A., Kwon, E.Y., Friedrich, T., 2020. Timing and magnitude of Southern Ocean sea ice/carbon cycle feedbacks. Proc Natl Acad Sci USA 117, 4498–4504. https://doi.org/10.1073/pnas.1908670117

Stephens, B.B., Keeling, R.F., 2000. The influence of Antarctic sea ice on glacial–interglacial CO_2 variations. Nature 404, 171–174.

Tagliabue, A., Sallee, J.-B., Bowie, A.R., Levy, M., Swart, S., Boyd, P.W., 2014. Surface-water iron supplies in the Southern Ocean sustained by deep winter mixing. Nature Geoscience 7, 314–320. https://doi.org/10.1038/ngeo2101

Therón, R., Paillard, D., Cortijo, E., Flores, J.-A., Vaquero, M., Sierro, F.J., Waelbroeck, C., 2004. Rapid reconstruction of paleoenvironmental features using a new multiplatform program. Micropaleontology 50, 391–395.

Thöle, L.M., Amsler, H.E., Moretti, S., Auderset, A., Gilgannon, J., Lippold, J., Vogel, H., Crosta, X., Mazaud, A., Michel, E., Martínez-García, A., Jaccard, S.L., 2019. Glacial-interglacial dust and export production records from the Southern Indian Ocean. Earth and Planetary Science Letters 525, 115716. https://doi.org/10.1016/j.epsl.2019.115716

Toggweiler, J.R., Russell, J.L., Carson, S.R., 2006. Midlatitude westerlies, atmospheric CO_2 , and climate change during the ice ages. Paleoceanography 21, n/a-n/a. https://doi.org/10.1029/2005PA001154

Tzedakis, P.C., Hooghiemstra, H., Pälike, H., 2006. The last 1.35 million years at Tenaghi Philippon: revised chronostratigraphy and long-term vegetation trends. Quaternary Science Reviews 25, 3416–3430. https://doi.org/10.1016/j.quascirev.2006.09.002

Ullermann, J., 2015. Glacial-interglacial oceanic changes in the central Pacific sector of the Southern Ocean during the past 500 ka (PhD Thesis). http://www. suub. uni-bremen. de.

Vázquez Riveiros, N., Waelbroeck, C., Skinner, L., Roche, D.M., Duplessy, J.-C., Michel, E., 2010. Response of South Atlantic deep waters to deglacial warming during Terminations V and I. Earth and Planetary Science Letters 298, 323–333. https://doi.org/10.1016/j.epsl.2010.08.003

Waelbroeck, C., Jouzel, J., Labeyrie, L., Lorius, C., Labracherie, M., Stiévenard, M., Barkov, N.I., 1995. A comparison of the Vostok ice deuterium record and series from Southern Ocean core MD 88-770 over the last two glacial-interglacial cycles. Climate Dynamics 12, 113–123.

Zondervan, I., 2007. The effects of light, macronutrients, trace metals and CO_2 on the production of calcium carbonate and organic carbon in coccolithophores—A review. Deep Sea Research Part II: Topical Studies in Oceanography 54, 521–537. https://doi.org/10.1016/j.dsr2.2006.12.004

Zweng, M., Seidov, D., Boyer, T., Locarnini, M., Garcia, H., Mishonov, A., Baranova, O., Weathers, K., Paver, C., Smolyar, I., 2019. World ocean atlas 2018, volume 2: Salinity.